DEVELOPMENT OF A

FIBRE OPTIC STRAIN GAUGE

FINAL REPORT BY:

M.D. Alpert
J.W. Snow
S.H. Woodside

FOCAL MARINE LIMITED

Work on the project was conducted under the auspices of the Canada Centre for Mineral and Energy Technology, Energy, Mines and Resources Canada.

DSS FILE NO.: 14SQ 23440-6-9183

DSS CONTRACT SERIAL NO.: 23440-6-9183/01-SQ

CANMET PROJECT NO.:

CANMET SCIENTIFIC AUTHORITY : D.K. Mak

49pp

DATE: October 23, 1987

MICROMEDIA

SUMMARY

The construction and evaluation of fibre optic strain gauges based on the microbending principle was undertaken. Three different methods of transferring strain to an optical fibre deformer were constructed and tested. It was concluded that a "Poisson Tube" gauge is the most promising method (although not the most sensitive in the present prototype) because it structurally incorporates good environmental sealing and possesses a theoretically high directional sensitivity. Gauge sensitivities of 0.02 dB/uϵ were achieved.

TABLE OF CONTENTS

LIST OF TABLES AND FIGURES iv

1.0 INTRODUCTION 1
1.1 PURPOSE 1
1.2 BACKGROUND 1
1.3 TEST BENCH DESIGN 2
1.4 HOUNSFIELD TENSOMETER 4
1.5 FIBRE SELECTION 4
1.6 LEAD FIBRE SELECTION 7
1.7 OPTICAL MEASUREMENT SETUP 7

2.0 GAUGE CONFIGURATIONS 9
2.1 MOLDED STRAIN GAUGES 9
2.2 HARMER-TYPE STRAIN GAUGE: 12
2.3 POISSON TUBE STRAIN GAUGE 15

3.0 CONCLUSIONS AND RECOMMENDATIONS 22
3.1 CONCLUSIONS 22
3.2 RECOMMENDATIONS FOR FURTHER WORK 23

4.0 REFERENCES 24

5.0 ACKNOWLEDGEMENT 26

APPENDIX "A" - STATEMENT OF WORK. 27

APPENDIX "B" - TECHNICAL PAPERS 28

LIST OF TABLES AND FIGURES

TABLE 1	TEST BEAM PARAMETERS	5

FIGURE 1	TEST BEAM	3
FIGURE 2	TEST BEAM CALIBRATION - STRAIN VERSUS LOAD	6
FIGURE 3	OPTICAL SET-UP	8
FIGURE 4	MOLDED GAUGES	10
FIGURE 5	HARMER TYPE GAUGES	13
FIGURE 6	HARMER TYPE GAUGE - CLAMPED ON AL BEAM	14
FIGURE 7	POISSON TUBE GAUGE	16
FIGURE 8	POISSON TUBE GAUGE - TENSOMETER TEST . .	18
FIGURE 9	POISSON TUBE GAUGE - EPOXY BOND ON STEEL BEAM - TEST 1	19
FIGURE 10	POISSON TUBE GAUGE - EPOXY BOND ON STEEL BEAM - TEST 2	20
FIGURE 11	POISSON TUBE GAUGE CREEP - EPOXY BOND ON STEEL BEAM	21

1.0 INTRODUCTION

1.1 PURPOSE

This report concludes contract DSS 23440-6-9183/01-SQ "Development of a Fibre Optic Strain Gauge". Presented herein are the experimental results of three different prototypes along with a description of test bench design. Also included for the background of the reader are copies of two of the more germane technical references.

1.2 BACKGROUND:

Intensity modulation induced by microbend loss in multimode fibres is well documented (1,2).

Sensors for strain and pressure utilizing the microbending principle have been previously described (3,4,5,6).

The purpose of this contract was to develop an engineering prototype of a small scale (1cm X 1cm) fibre optic strain gauge based on the microbending principle. (The Statement of Work is presented in Appendix "A".)

Microbending resulting in intensity modulation was the method selected as this method employs inexpensive sources and detectors, and fibre displacement in the sub-angstrom range are reported (1), albeit using sophisticated instrumentation.

The Statement of Work outlined four objectives (a-d; see Appendix "A"). These objectives were treated in the following manner:

a) Early in the work it became obvious that any fibre configuration would require packaging which would itself seal the fibre from a particular operating environment. Without some form of protective packaging, environmental conditions could affect fibre durability or optical properties. The need to test the fibre in immersion under pressure was therefore no longer required.

b) Earlier in-house work evaluated various fibre geometries that would perform microbending. Only a corrugated structure was adaptable for strain measurement in a manner similar to metal foil type gauges.

c) Various methods of corrugated structure

displacement mechanisms were investigated and the resulting sensors were characterized. Some of these methods have more desirable packaging configurations for environmental sealing.

d) Various configurations were characterized by developing optical power versus microstrain response curves. Repeatability was addressed but limits of elastic bending, effect of cycling on fatigue, effect of environmental noise and long term reliability could not be addressed at this early stage.

1.3 TEST BENCH DESIGN:

Sensor configurations developed during this contract were evaluated by bonding them to a test beam. The beam was then loaded with weights to induce various strain levels.

Important parameters in the design of the test beam were:

a) The beam dimensions should be small to keep force required for maximum strain small; this would minimize the number and size of laboratory weights required (tensile or compressive strain induced without bending would require numerous laboratory weights).

b) The beam cross sectional area should be large enough so that gauge would not appreciably add to beam strength.

c) Both tensile and compressive strains should be easily achieved.

d) The maximum achievable strain should be 2000 microstrain with a 4000 microstrain proportional limit for shock when loading weights.

e) The beam should provide an area of constant strain (test area) suitable for the gauge geometries to be tested.

Figure 1 shows the actual test beam construction and dimensions. An end supported beam loaded at two intermediate points provides an area between the loading points of constant strain. A gauge affixed to the beam experiences tensile strain when on the lower surface and compressive strain on the upper surface; once a gauge is affixed the

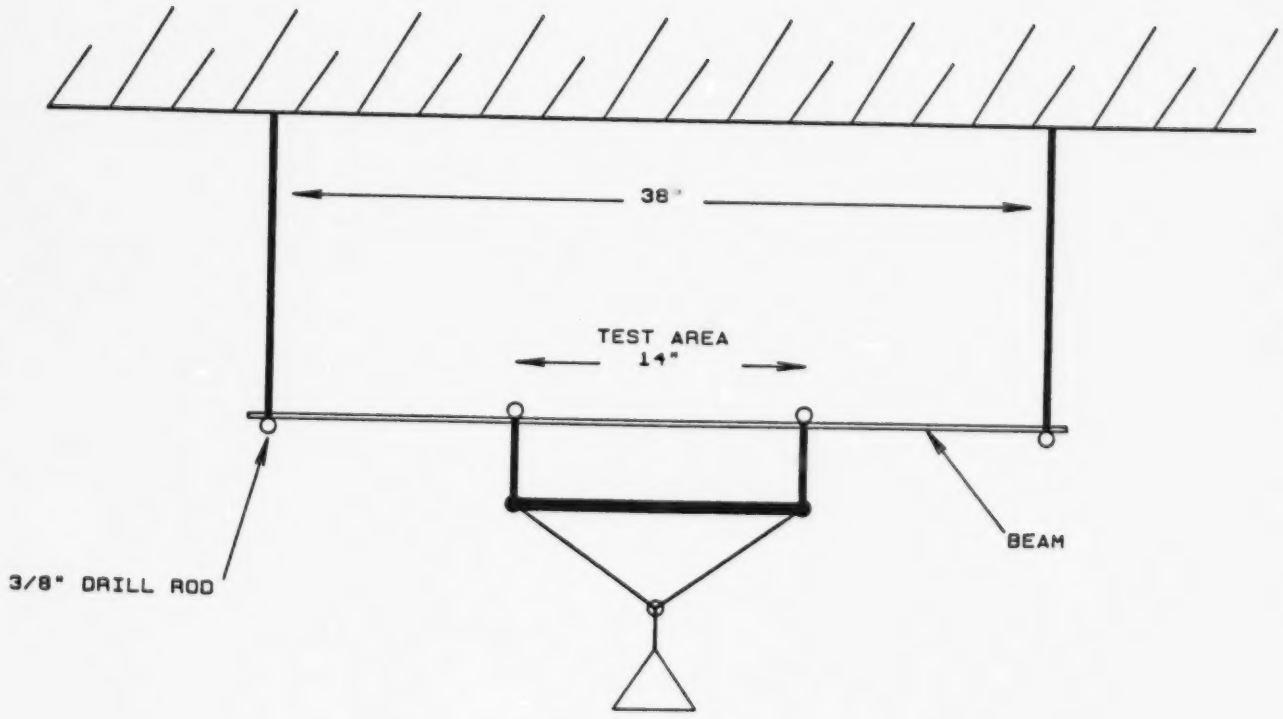

FIGURE 1 - TEST BEAM

change between tensile and compressive testing is easily achieved by inverting the beam.

Two beam materials were used. Their specifications are as follows:

Material: 6061-T6 Aluminum
thickness = 6.35mm (1/4")
Width = 50.8mm (2")
Length = 101.6cm (40")
Distance between end supports
= 96.5cm (38")
Distance between loading points
= 35.6cm (14")
Material: Mild Steel
thickness = 3.2mm (1/8")
other dimension same as for Aluminum above.

The Aluminum beam provides a larger strain range while the steel beam permits gauge bonding by spot welding.

Table 1 lists the beam parameters. Figure 2 shows the relationship between weight suspended from the spreader and strain induced in the test area (as calculated from formulae presented in Table 1).

1.4 HOUNSFIELD TENSOMETER:

To test a specimen under tensile strain, without any of the bending effects produced by the test beam, a Hounsfield Tensometer (7) was used.

1.5 FIBRE SELECTION:

A polyimide coated fibre (FHP 100/120/140) from Polymicro Technologies (8) was the fibre of choice for all tests. The thin hard coating of Polyimide (thickness = 10um) communicates the applied force to the glass fibre more efficiently than do more common softer buffers.

The fibre specifications are:

Core:	100 microns
Cladding:	120 microns O.D.
Polyimide Buffer:	140 microns O.D.
Core Refractive Index:	1.4533 at 800 nm.
Clad Refractive Index:	1.44 at 800 nm.
Numerical Aperture:	0.22 = +/- 0.02
Index Profile:	Step

TABLE 1 TEST BEAM PARAMETERS

Aluminum Beam	Steel Beam
ϵ = 28.8 E-6/lb*W	ϵ = 38.4 E-6/lb*W
Wmax = 122 lbs	Wmax = 31.3 lbs
ϵ max = 3500 E-6	ϵ max = 1200 E-6
δ max = 4.4"	δ max = 3"

Derivation:

$\epsilon = yM/EI$

$M = xP$

$I = (bh^3)/12$

therefore:

$$\epsilon = \frac{(h/2)(x*W/2)}{E*(bh^3)/12}$$

M = bending moment
E = modulus of elasticity
y = distance from neutral axis (=h/2)
I = moment of inertia
b = beam width
h = beam thickness
x = moment arm
P = force (P/2=W; W = weight applied at each of 2 points)

The above values represent theoretical calculations of test beam parameters upon which fibre optic strain gauge prototypes were tested. Since no testing was performed to verify these parameters notes on errors based on beam material variability is presented below:

a) The non-linearity for the aluminum beam loaded from 0 to 70 lbs. and for the steel beam loaded from 0 to 30 lbs. is estimated at less than 5% (The curvature of the beam between the two loading points, test region, is only approximately uniform. This non-linearity results in a departure from constant strain in this region).

b) Errors in material properties such as Young's Modulus, E, may be as great as 10% but this affects only absolute values.

c) Repeatability is only insignificantly affected by the positioning of the beam end supports and the positioning of the two loading points. Repeatability within 2% is estimated.

FIGURE 2 – TEST BEAM CALIBRATION

(strain vs. load)

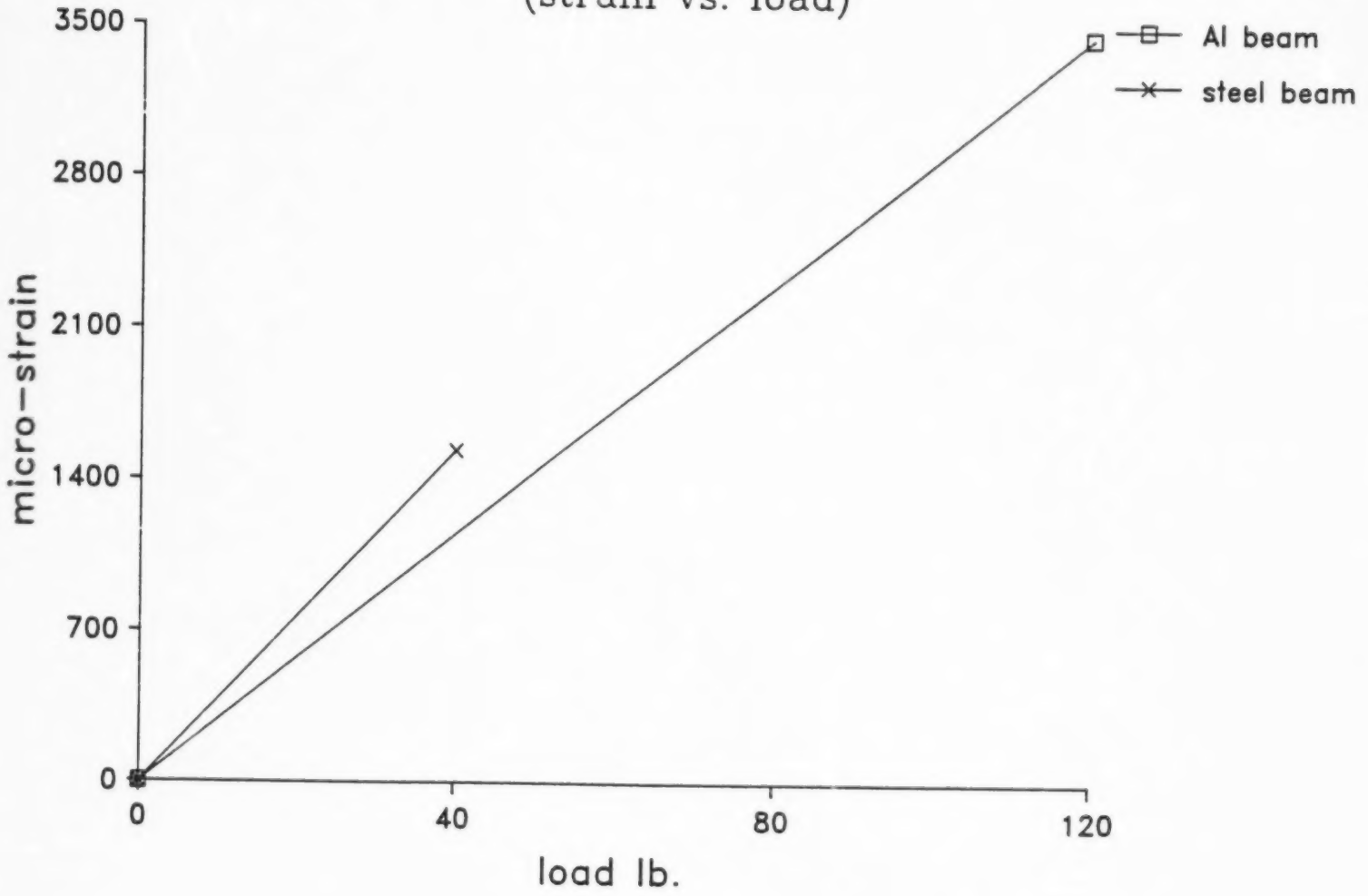

The optimum periodicity (c) from maximum microbending attenuation (1) was calculated to be:

$$\Lambda_c = \frac{|2 * (pi)(100E\text{-}6M)(1.4533)}{0.22}$$

$$\Lambda_c = 2.93E\text{-}3 \text{ m}$$

i.e.,

$$= 2.93 \text{ mm} +/- 0.3 \text{ mm}$$

A periodicity of 3.2 mm used. This difference in periodicity from the optimum should have no significant effect because:

a) it is within the percentage uncertainty (this periodicity was calculated on our best assumption of the numerical aperture which was not accurately known early in the work);
b) sensitivity versus periodicity has a broad peak about the critical periodicity (1);
c) the calculated value for the critical periodicity of a specific fibre is generally smaller than the experimentally obtained value (1).

1.6 LEAD FIBRE SELECTION:

To minimize macrobending and microbending effects in the lead fibre Corning Corguide Graded Index Fibre (100/140) was used. The matching core sizes assure minimal loss splices while the change to a larger N.A. (Corguide N.A. = 0.29) caused rejection of the higher order modes from the lead fibres where either microbending (mode coupling to the radiated modes) or macrobending have the greatest effect (9). To minimize any losses due to these effects the lead fibres were always kept reasonably straight or bent in large arcs of radii greater than 10 cm.

1.7 OPTICAL MEASUREMENT SETUP:

The Optical Measurement Test Instrumentation is outlined in Figure 3.

A Scrambler-Stripper provides an equilibrium mode distribution and removes cladding modes. In this early developmental work, no differences were noted in the experimental results when the scambler-stippers were present and thus these components were not always used.

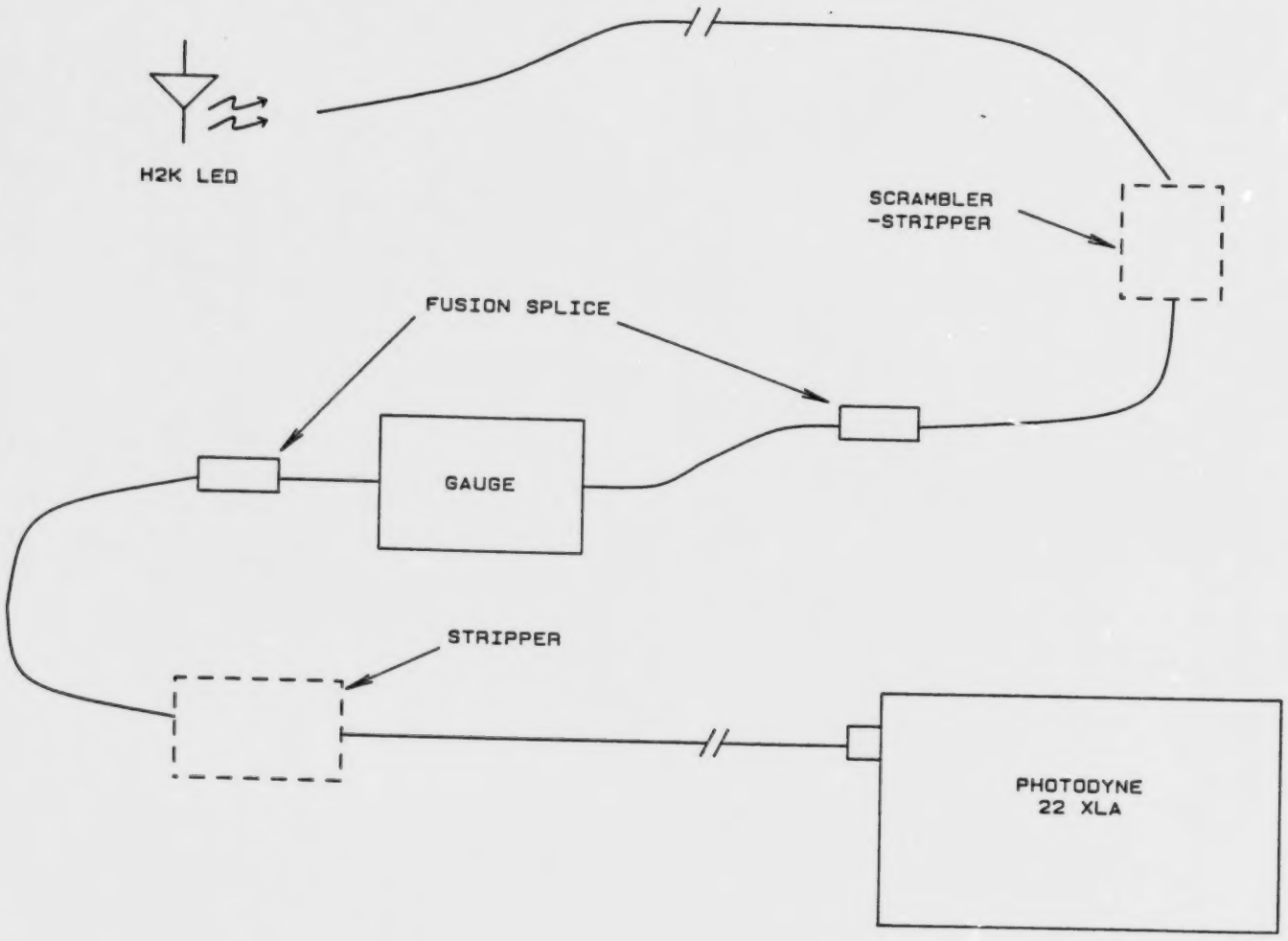

FIGURE 3 - OPTICAL SET-UP

2.0 GAUGE CONFIGURATIONS

2.1 MOLDED STRAIN GAUGES:

An attempt was made to produce a Strain Gauge by encapsulating fibres in a material that could be bonded to an object under strain (Figure 4). The intent was to encapsulate the fibres in a weave which provided an offset attenuation that was sensitive to both tensile and compressive strain. The possibility of Plasma spraying fibres was discussed (9) but the temperatures involved made it impossible with present day buffer materials.

Construction:

The encapsulant selected was an epoxy resin:
Struers Epofix Resin and Hardener
Copenhagen, Denmark
(8 parts resin: 1 part hardener)

Molds were constructed of teflon for ease of material removal. Gold plated pins of 1.0 mm diameter were press fitted into the lower mold body from the underside. Polyimide coated fibre was woven around the pins in various configurations. The pins were extracted before total resin cure.

The points at which fibre entered the encapsulant required some form of strain relief. Initially a brass tube of approximately 1.5 mm. O.D. was used to which a loose tube cable jacket was affixed. This "large" diameter brass tube often broke away from the encapsulant during gauge removal from the mold. A flexible rubber tubing was later used with more success. The final thickness of the gauge would likely be limited by this structure.

The molding process produced a thicker edge due to the liquid resin meniscus. This edge was milled down to produce a gauge approximately 2 mm. thick.

The encapsulant was affixed to the beam with cyanoacrylate adhesive and tested.

Results:

Results were inconclusive, that is, there was no significant relationship between the strain applied and attenuation noted. The cyanoacrylate bond between the gauge

MOLD 1 :

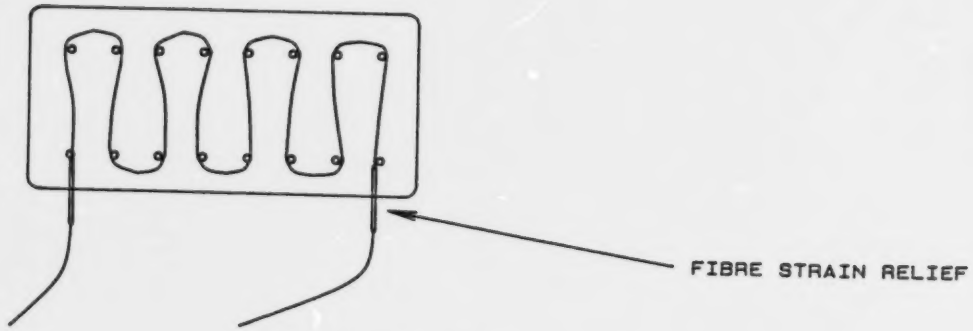

DEFORMER PERIOD = 12.25 mm

PIN DISPLACEMENT = 15 mm

ENCAPSULANT THICKNESS = 2.5 mm

MOLD 2 :

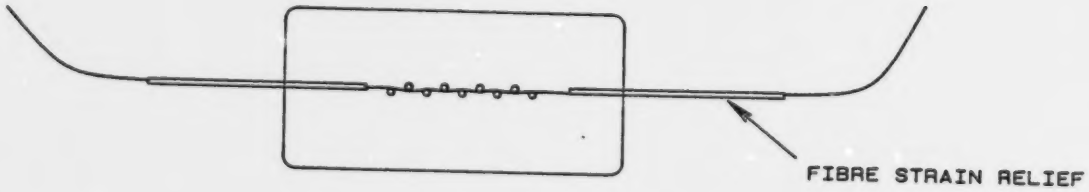

DEFORMER PERIOD = 5.0 mm

PIN DISPLACEMENT = 0.75 mm

ENCAPSULANT THICKNESS = 2 mm

FIGURE 4 - MOLDED GAUGES

and the beam was found to be suspect in other gauge configurations and thus requires further testing here. However, the discussion below indicates that any further efforts are not warranted for this configuration based on sensitivity arguments.

Discussion:

The sensitivity of this type of gauge depends in part on the fibre weave orientation during bonding. If bonded so that the strain to be measured is parallel to the longer axis of the weave (Figure 4), the largest effect should be an amplitude change due to the poisson effect i.e., the contraction occurring perpendicular to the direction of applied strain; a change in periodicity should result but would offer minimal signal change (Such an orientation would result in a gauge with questionable directional sensitivity). If bonded in the other plane fibre displacement would take place causing attenuation changes. This orientation would also result in minimal sensitivity because the gauge length can be no more than the fibre peak to peak amplitude. Mold 2 (Figure 4) has a pin displacement of 0.75 mm which results in a fibre displacement of 390 um (Pin displacement is a measure of the center to center offset of the two rows of pins. Fibre displacement can be calculated from pin displacement).

If:

$$\epsilon = dL/L$$

(dL = change in length)
(L = original length)

the amplitude of fibre perturbation, A, will be changed by

$$dA = A$$

If A = 390 um, for 1 μ :

$$dA = (1E\text{-}6)(390\mu m)$$

$$dA = 3.9E\text{-}4\mu m.$$

This small displacement would results in very low gauge sensitivity. For example, even with strain levels of 1000 u the displacement is only 0.39um. Based on results using the Harmer-Type Gauge (below), which achieved a sensitivity of 0.2 dB/um (calculated from strain and gauge length), this would give a signal change for a 1000 u range of:

$$(0.2\ dB/\mu m)(0.39\mu m) = 0.078dB.$$

A range of 0.078 dB over 1000 με is too small for practical resolution.

Also, gauge construction of this type would likely suffer from lack of uniformity between gauges. The holes left after pin removal present a material discontinuity; if filled the material would not be cross linked to the main mass.

2.2 HARMER-TYPE STRAIN GAUGE:

A gauge which translates the relative movement between two points in a material under stress to one point, usually central, has been described by Harmer (5).

The displacement required to operate a microbend type sensor is a function of the distance between these two points; this is essentially a measure of the gauge length.

Construction:

A gauge was constructed as shown in Figure 5. The deformer plates provided for 12 periods of 3.2 mm periodicity. The gauge was mounted on the aluminum test beam using small C-clamps.

Results:

Figure 6 shows typical results obtained with this gauge. Good sensitivity on the order of 0.02 dB/micro-strain and good repeatability were shown.

The following tests details apply to Figure 6:

Test 1: 0 dB = -35.7 dBm; increasing strain levels.
Test 2: 0 dB = -36.5 dBm; decreasing strain levels; performed 5 hrs after test 1.

The cause of the level shift between test 1 and test 2 was not determined and could likely be source drift.

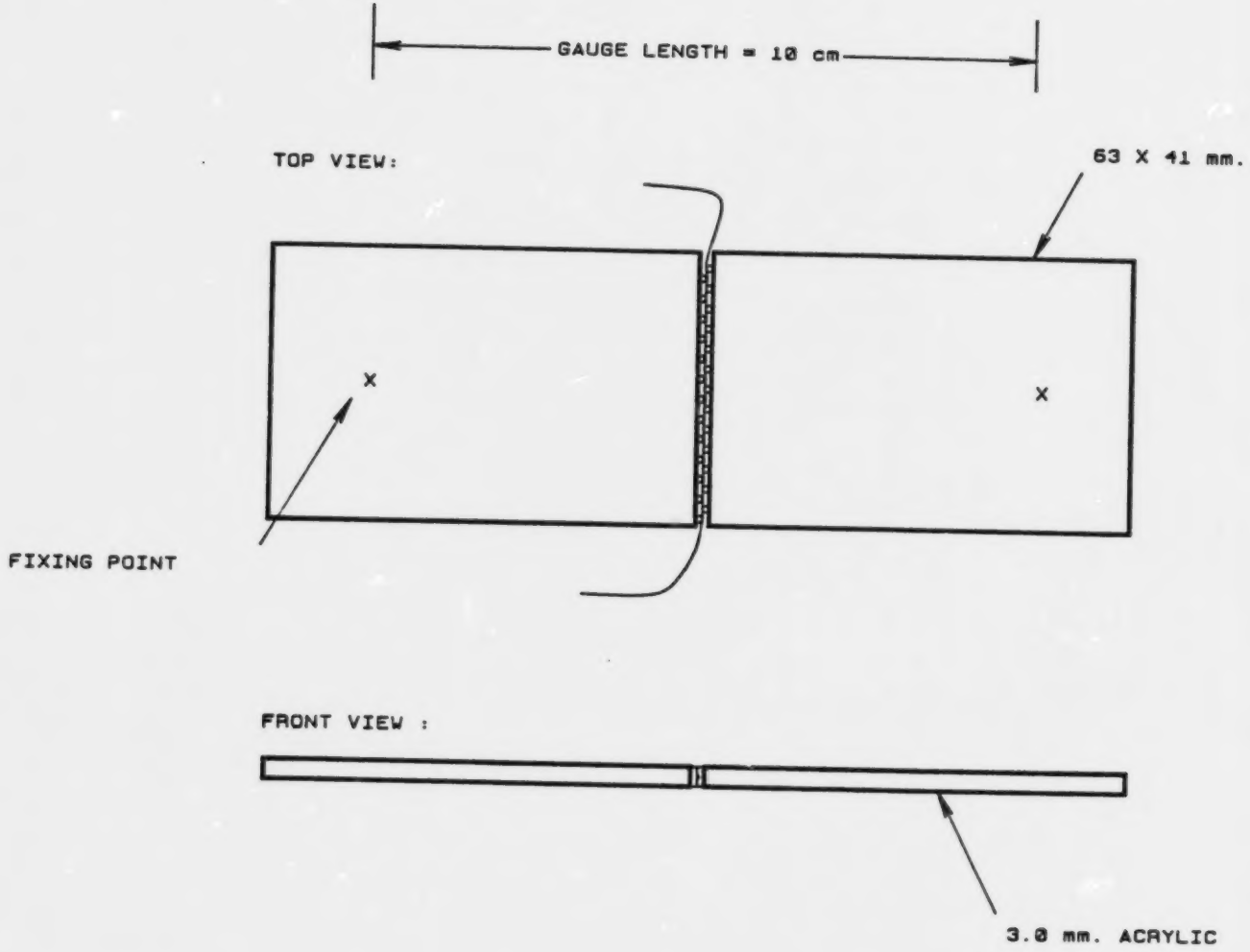

FIGURE 5 - HARMER TYPE GAUGE

FIGURE 6 – HARMER TYPE GAUGE

(clamped on Al beam)

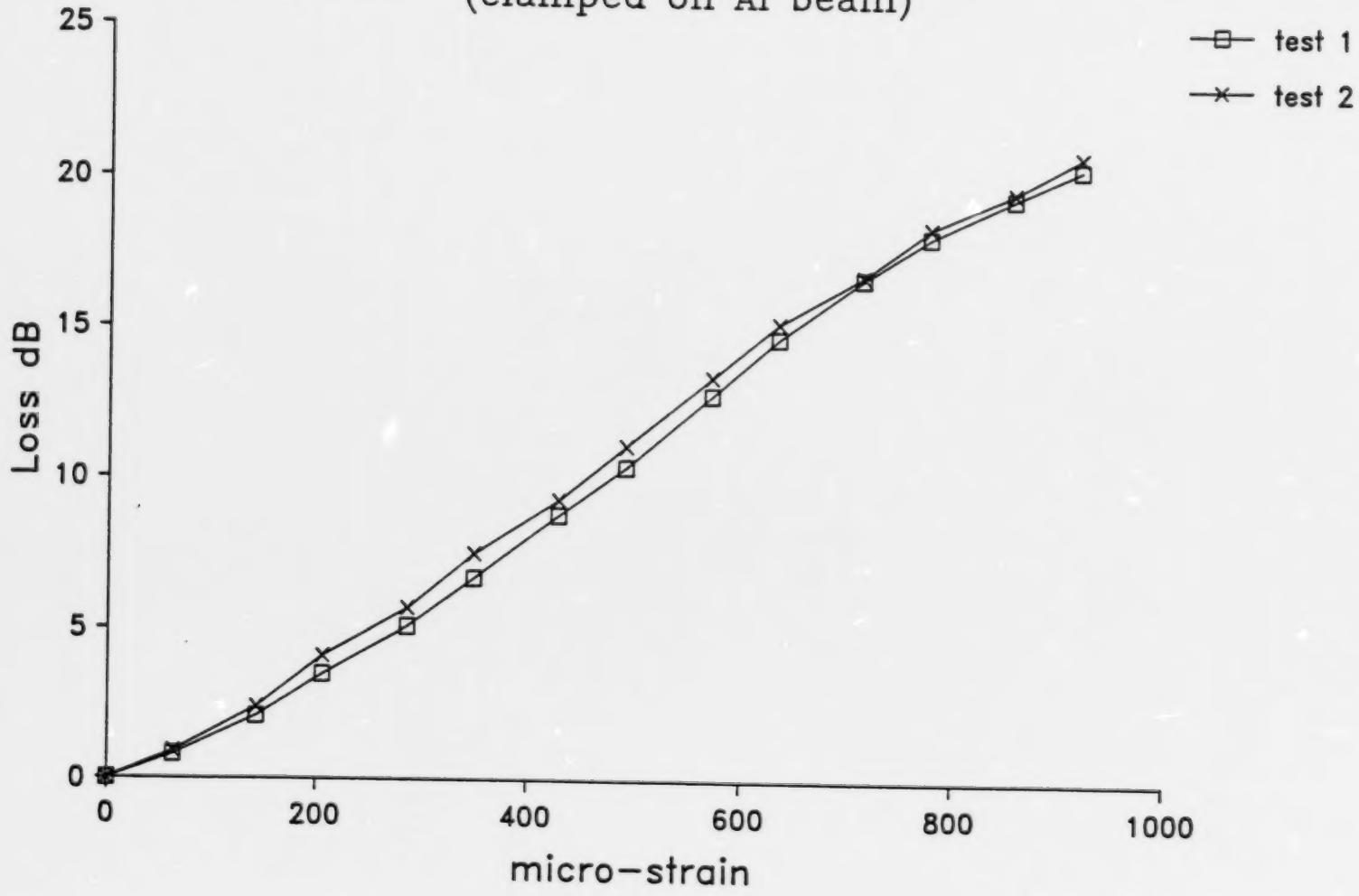

Discussion:

Although the sensitivity of this gauge was excellent the displacement transfer mechanism does not lend itself to simple environmental sealing.

2.3 POISSON TUBE STRAIN GAUGE:

A material under strain will change dimensions in a plane perpendicular to the induced strain as defined by the Poisson ratio. A thin tube spot welded to a thin base material along their line of contact can produce a weldable strain gauge; the active element, a fibre optic microbender inserted into the tube, can sense the diameter change of the tube (10).

There are two advantages of such a gauge:

a) The tube provides isolation of the fibre from harsh environments.

b) The narrow gauge weld line provides for a good directional sensitivity.

Tube diameter change with varying strain will not be uniform because the applied stress is transferred from base to tube only through the one weld line. It is assumed that this non-uniformity is small enough to be ignored in the present study.

Construction:

Figure 7 illustrates the layout and dimensional details for this gauge.

Stainless steel shim stock (0.13mm) and stainless steel tube (diameter = 9.5 mm, wall thickness = 0.3mm) were welded together along their line of contact with a spot welder (11). PVC Rod was filed into two half-cylinders and steel rods of 0.9 mm diameter were attached. The resulting deformer had 9 microbending sites (periods) of periodicity = 3.2 mm.

The dimensional tolerances to place the deformer unit within the tube were critical and at present always require shims. Keeping the fibre in position, in the centre of the deformers, requires adhering the fibre to the end deformer rods with a compliant adhesive such as RTV silicone.

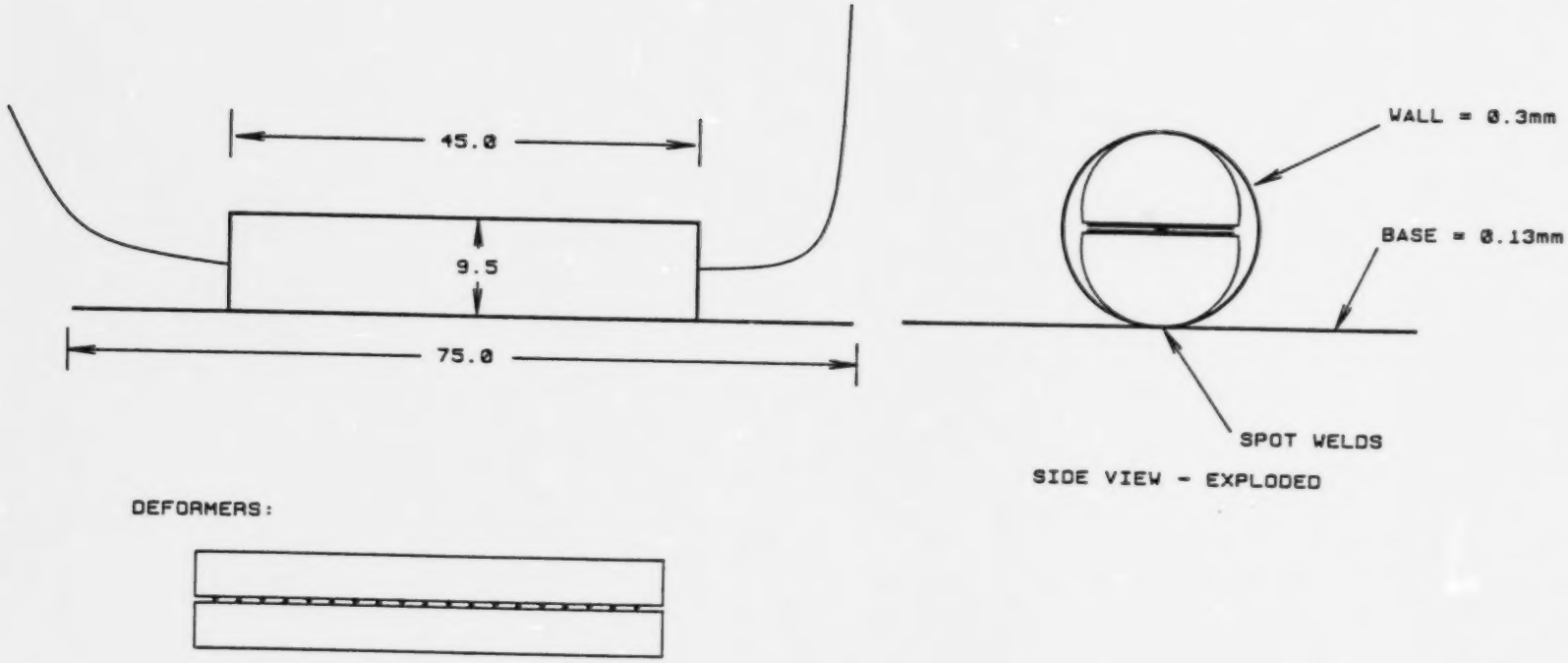

FIGURE 7 - POISSON TUBE GAUGE

Results:

The initial tests were made on the Hounsfield Tensometer (Figure 8). The gauge base itself was stressed between the tensometer jaws to eliminate any question of bonding the gauge to a substrate. Initial sensitivity was calculated at 0.003 dB/$\mu\epsilon$.

The gauge was then spot welded to the steel test beam but proper welds were not achieved and the gauge broke away under test. The gauge was later epoxied to the steel beam using Tra-Con Epoxy Adhesive F-113. Testing (Figure 9) reveals a sensitivity of 0.003 dB/$\mu\epsilon$. Further testing (Figure 10) shows hysteresis and decreased sensitivity. The hysteresis is possibly due to weakening of the beam-gauge bond. To prove this a time study (Figure 11) of gauge stability (under a full load followed by no load) was carried out. The indication is that the epoxy bond fails with time which causes the transfer of strain to the gauge to be relieved.

FIGURE 8 – POISSON TUBE GAUGE

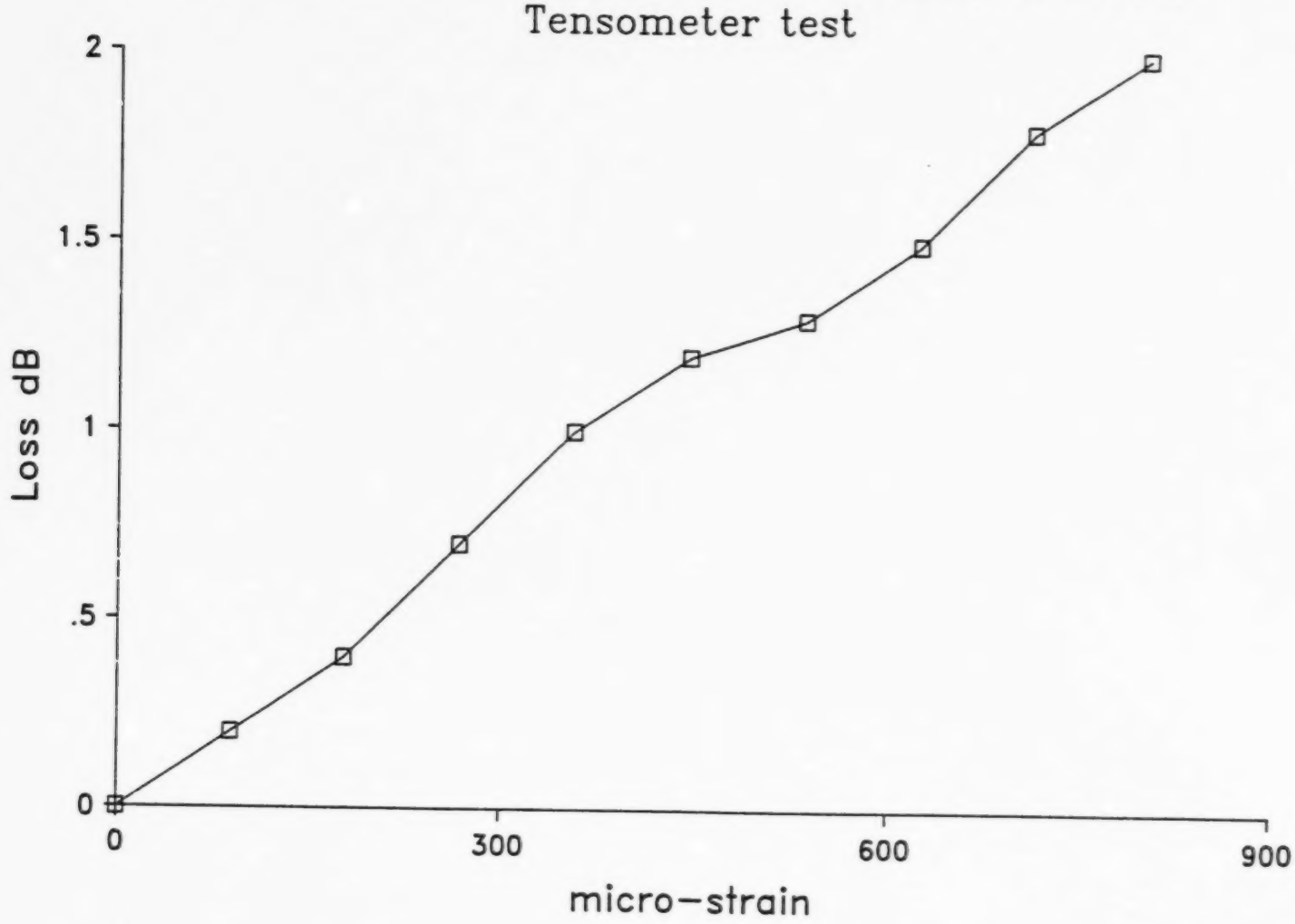

FIGURE 9 – POISSON TUBE GAUGE

(epoxy bond on steel beam – test 1)

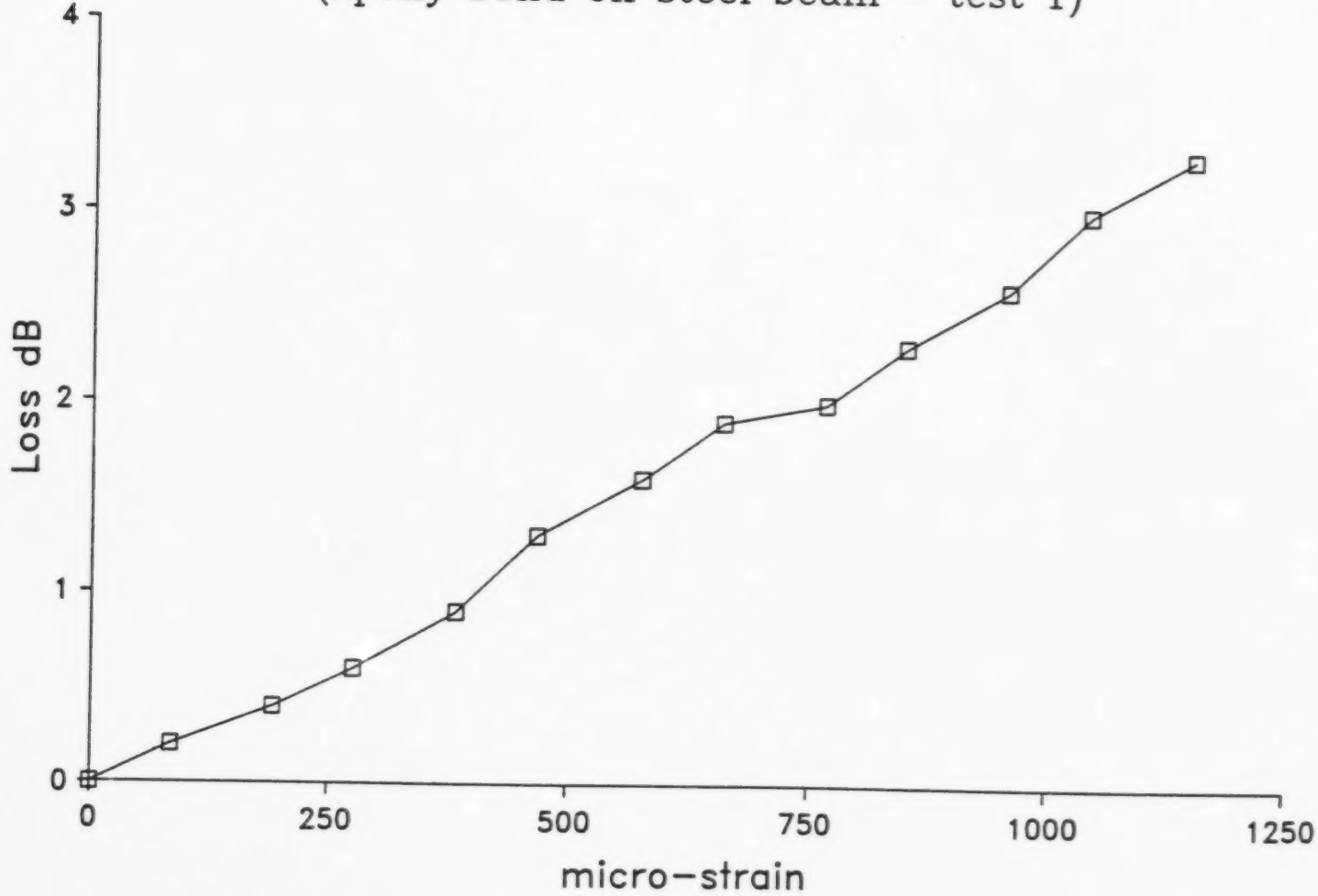

FIGURE 10 – POISSON TUBE GAUGE

(epoxy bond on steel beam – test 2)

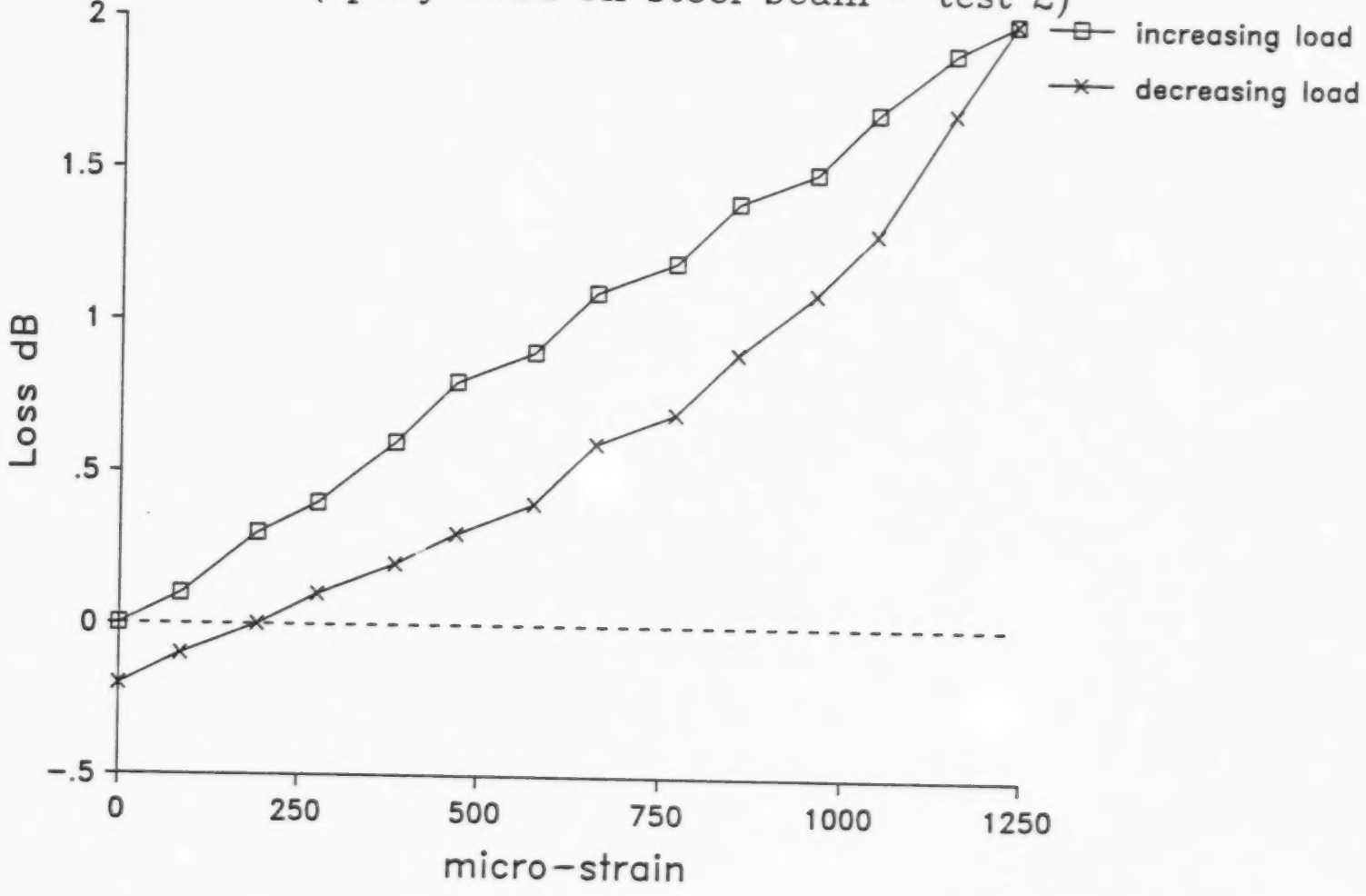

FIGURE 11 – POISSON TUBE CREEP

(epoxy bond on steel beam)

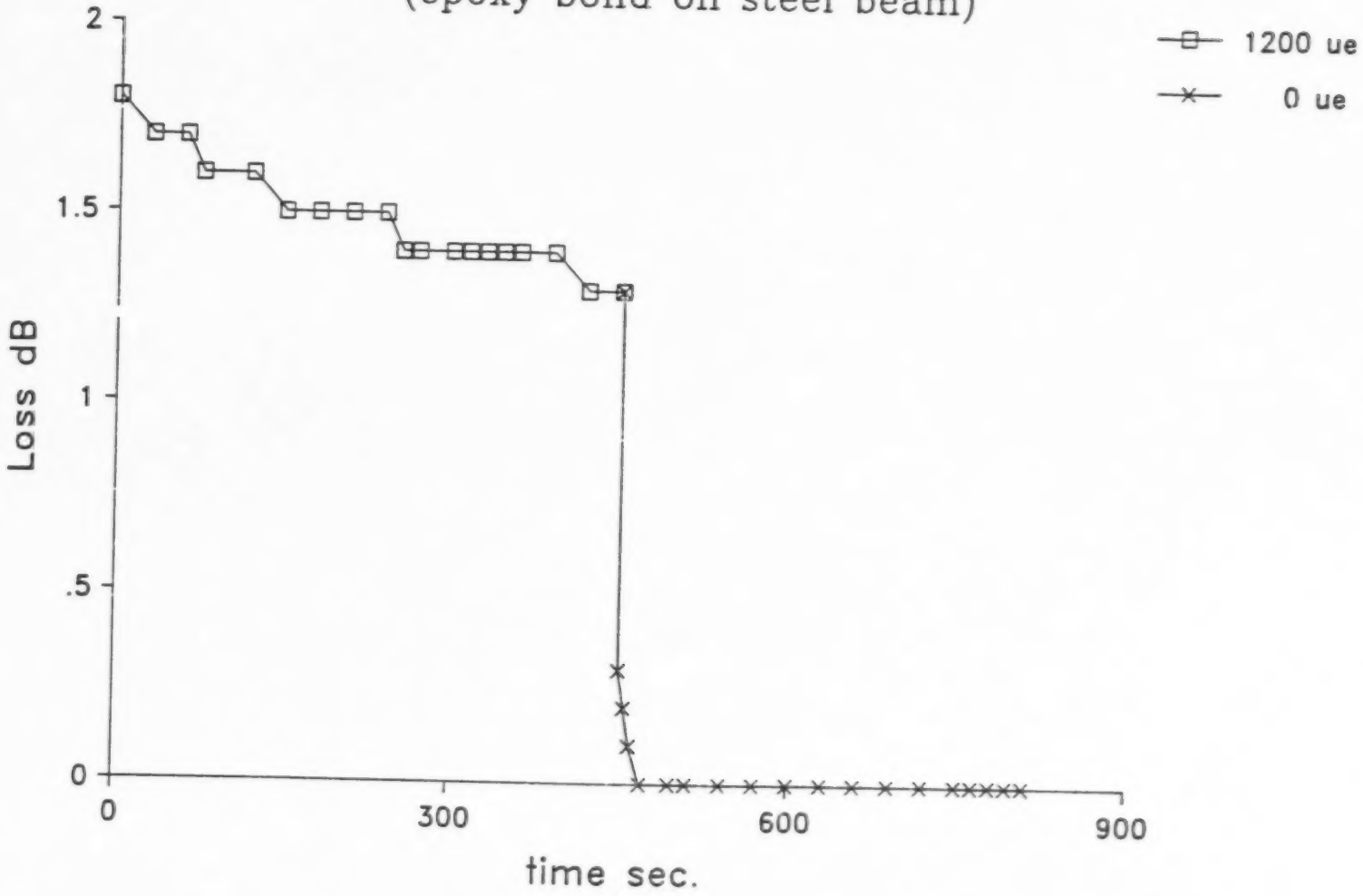

3.0 CONCLUSIONS AND RECOMMENDATIONS

3.1 CONCLUSIONS:

Polyimide coated fibre, while sensitive to microbending, was very difficult to handle. We question its long term reliability. It appears that the hard thin coating is easily scored which results in fibre breakage.

Gauge bonding, as with all strain gauges, was found to be critical to gauge function. This is especially critical because of the "robustness" of the prototypes studied here.

The Harmer-type strain gauge provided the best sensitivity of all gauges studied but does not readily lend itself to simple packaging. Packaging would require an extremely compliant covering over two very rigid plates (or sets of arms). These plates must slide over the substrate to translate the relative motion at the two "fixing" points to the centrally located fibre. The plates must, however, be rigidly fixed to the substrate at the fixing points.

Although the molded gauges were insensitive to strain in the present configuration the similarity between them and the sensitive Harmer type means the design could be altered to effectively increase gauge length. A combination molded and Harmer-type would likely be a workable alternative.

The Poisson tube did not equal the sensitivity of the Harmer-type gauge (0.003 dB/$\mu\epsilon$ versus 0.02 dB/$\mu\epsilon$ respectively); sensitivity improvements would result with optimization of gauge construction. However, the Poisson tube gauge design is advantageous because:

a) it lends itself to simplified packaging by the very nature of its construction and

b) it theoretically possesses a low transverse sensitivity (good directional sensitivity).

There was some concern that during the present work a portion of the stated sensitivity may actually be due to bending of the tube caused by bending of the beam. The tensometer test (Figure 8), where bending effects were minimized, showed that this was not a major factor.

3.2 RECOMMENDATIONS FOR FURTHER WORK:

The success with the Poisson tube gauge and the fact that harsh environment type electrical gauges of similar construction (12) are well established makes it a candidate for further investigation.

All future work should be directed toward a specific application, i.e., exactly where the gauge will be used, what kinds and levels of strain it will experience, what environmental factors it will be subjected to. Once these are identified future work would involve:

a) Selecting a fibre that is both sensitive to microbending but has good wear and cycling characteristics.

b) An analysis of tube deformation when under strain. This will involve a literature search directed, for the most part, at similarly constructed electrical type gauges, and, if required, a photo-elastic analysis of the present configuration under both tensile and compressive strain.

c) Optimization of base-tube construction for maximum tube deformation.

d) A study of deformer design suited to tube deformation characteristics.

e) Improvements in gauge bonding. Research into and adoption of procedures used for weldable electrical type gauges. Determining that gauge bonding does not contribute to hysteresis.

f) A study of other possible materials for gauge construction that would extend its usefulness to non-weldable applications.

g) An evaluation facility that would employ metal foil gauges for reference and comparison.

4.0 REFERENCES

1. Nicholas Lagakos, J.H. Cole, and J.A. Bucaro. Microbend fiber-optic sensor. Applied Optics Vol. 26, No. 11, 1 June, 1987. pp 2171-2180.
(A copy of this paper is included in appendix "B")

2. Kevin E. Lindsay and Barry E. Paton Wide Range Optical Fibre Microbending Sensor, SPIE Conference # 611. Quebec City, Quebec. June, 1986. pp. 211-217.
(A copy of this paper is included in appendix "B")

3. N. Lagakos, W.J. Trott, T.R. Hickman, J.H. Cole, and J.A. Bucaro, Microbend Fiber-Optic Sensor as Extended Hydrophone, IEEE J. Quantum Electron. QE-18, 1633 (1982).

4. J.A. Bucaro, J.H. Cole, A. Dandridge, T.G. Giallorenzi, and N. Lagakos. Fibre Optic Acoustic Sensors. SPIE Vol 661. Optical Testing and Metrology (1986).

5. Harmer, Alan L., Inventor. United States Patent 4,163,397; August 7, 1979. Optical Strain Gauge. Assigned to Battelle Development Corporation, Columbus, Ohio.

6. K. Spenner. Microbending pressure and displacement sensor. Paper THGG10. OFS (Conference on Optical Fibre Sensors, 14 February, 1987)

7. Tensometer Limited, Croydon, England. Serial No. W6592.

8. Polymicro Technologies
   3035 N. 33rd. Drive
   Phoenix, Arizona
   U.S.A. 85017

9. Dr. Gordon Murphy, Department of Engineering Physics, Technical University of Nova Scotia, Halifax, Nova Scotia.

10. The initial idea for construction of such a gauge came from Mr. W.K. Morrison, P.Eng., Director, C-FER Atlantic (Centre for Frontier Engineering Research - Atlantic) TUNS Campus, Halifax, Nova Scotia

11. UNITEK Spot Welder 1-312-13
(Settings: Pulse = 1; Heat = 198 watt-seconds).

12. Eaton Corporation
Transducer Products
2238 Alaska Avenue
El Segundo, California
U.S.A. 90245-4896

5.0 ACKNOWLEDGEMENT

We gratefully acknowledge the support of the Canada Centre for Mineral and Energy Technology, Energy, Mines and Resources Canada for financial assistance to carry out the work presented herein.

This work is a continuation of FOCAL MARINE LIMITED's internally funded research and development program into fibre optic measurement of strain, pressure and load.

APPENDIX "A"

STATEMENT OF WORK

Develop an engineering prototype of a small scale (1cm x 1cm) fibre optic stress/strain sensor based on the microbending principle. This sensor will use Corning Corguide step - index fibre or any other fibre as sensitive.

a) Test the selected fibre in immersion under pressure.

b) Evaluate the capability of various fibre geometries (corrugated structure, ellipsoidal helix, compressive helix) to measure compressive, tensile, bending and torsional types of strain.

c) Select appropriate housing materials for the fibre and for bonding to the glass gauge and to the structure to be measured. Access the effect of temperature (0 to 20 C), of vibrations (to 10 MHz and 2 g) and humidity.

d) Characterize the sensor: establish its response curve, the limits of elastic bending, the effect of fatigue on cycling, the effect of environmental noise, its repeatability and its long term reliability.

APPENDIX "B"

TECHNICAL PAPERS

Microbend fiber-optic sensor

Nicholas Lagakos, J. H. Cole, and J. A. Bucaro

Intensity modulation induced by microbending in multimode fibers is considered as a transduction mechanism for detecting environmental changes such as pressure, temperature, acceleration, and magnetic and electric fields. A generic microbend sensor has been defined and studied, and its components, such as sensing fiber, light source, optical fiber leads, and detector, have been examined and optimized. Finally, the generic microbend sensor has been tested demonstrating good performance.

I. Introduction

Extensive research has been directed toward development of fiber-optic sensors based on either phase or intensity modulation.[1,2] Intensity modulation induced by microbending loss in multimode fibers can be utilized as a transduction mechanism for detecting environmental changes. Specific microbend sensor designs have been already utilized for detecting pressure[2,3] and displacement.[4] In the latter sensor,[4] the threshold detectability level was limited by excess laser noise. In addition, the coherence of the laser introduced significant modal interference which resulted in lead instability.

In this paper, the generic microbend sensor is examined in detail. First, the microbending effect is studied in step and graded multimode fibers, and fiber designs maximizing the microbending sensitivity are presented. Light sources which can be used are considered, and their performance is evaluated. Lead problems are also discussed, and solutions are given minimizing significantly lead noise and sensor instability. The possible detection schemes are presented, and their complexity and advantages are examined. Then the generic microbend sensor is tested in detecting displacement, and its performance is presented. Finally, based on the generic sensor performance, the predicted minimum detectable environmental changes, such as pressure, temperature, acceleration, and magnetic and electric fields, are given.

The authors are with U.S. Naval Research Laboratory, Washington, DC 20375-5000.

Received 13 December 1986.

II. Generic Fiber Microbend Sensor

Consider an idealized generic microbend sensor as depicted in Fig. 1. The sensing fiber, which is sandwiched between a pair of deformer plates, is somehow constrained to bend in a regular pattern with periodicity Λ. The deformer, in response to an appropriate environmental change ΔE, applies a force ΔF to the bent fiber causing the amplitude of the fiber deformation X to change by an amount ΔX. The transmission coefficient for light propagating through the bent fiber T is in turn changed by an amount ΔT so that

$$\Delta T = \left(\frac{\Delta T}{\Delta X}\right) D \Delta E, \tag{1}$$

where

$$D\Delta E = \Delta X. \tag{2}$$

Here D is a constant which depends on the environment change ΔE. In terms of the applied force ΔF, Eq. (1) becomes

$$\Delta T = \left(\frac{\Delta T}{\Delta X}\right) \Delta F \left(K_f + \frac{A_s Y_s}{l_s}\right)^{-1}. \tag{3}$$

where k_f is the bent fiber force constant and $A_s Y_s/l_s$ is the force constant involved with changing the length of the deformer spacers. Here A_s, Y_s, and l_s are the cross-sectional area, Young's modulus, and length of the deformer spacers. The coefficient $\Delta T/\Delta X$, which relates the change in transmission to the change in fiber deformation amplitude, depends on the modal properties of the fiber and is discussed in some detail later. The change in optical transmission through the bent fiber results in a change in optical energy incident on the photodetector. The change in the photodetector output signal is thus used to detect the original environmental perturbation ΔE.

Depending on the construction of the deformer, various environmental parameters can in principle be sensed. The deformer converts the change in the envi-

ronmental parameter ΔE to a force ΔF on the bent fiber, i.e.,

$$\Delta F = \Delta E C.$$

For the generic deformer depicted in Fig. 1, the parameter C can be expressed as a simple function of deformer parameters for the various environmental sensors.

For a pressure sensor, C is simply equal to the area of the deformer plate A_p. Thus Eq. (3) becomes

$$\Delta T = \frac{\Delta T}{\Delta X} \cdot A_p \left(K_f + \frac{A_s Y_s}{l_s} \right)^{-1} \Delta P, \tag{4}$$

where ΔP is the change in pressure. Thus a high sensitivity pressure sensor should have $A_s Y_s / l_s$ small so that the effective compliance is determined by that of the bent fiber which is itself quite large. In this case Eq. (4) becomes

$$\Delta T \simeq \frac{\Delta T}{\Delta X} \cdot A_p k_f^{-1} \Delta P. \tag{5}$$

For a temperature sensor, C is equal to $A_s \alpha_s Y_s$, where α_s is the thermal expansion coefficient of the spacers. Then from Eq. (3)

$$\Delta T = \frac{\Delta T}{\Delta X} \cdot A_s \alpha_s Y_s \left(k_f + \frac{A_s Y_s}{l_s} \right)^{-1} \Delta \theta, \tag{6}$$

where $\Delta \theta$ is the temperature change. For a sensitive temperature sensor, Eq. (6) implies that one should have $k_f l_s \ll A_s Y_s$. In this condition Eq. (6) becomes simply

$$\Delta T \simeq \frac{\Delta T}{\Delta X} \cdot \alpha_s l_s \Delta \theta. \tag{7}$$

For a uniaxial accelerometer, the constant C is simply the mass of the deformer plate m_p. Equation (3) then becomes

$$\Delta T = \frac{\Delta T}{\Delta X} \cdot m_p \left(k_f + \frac{A_s Y_s}{l_s} \right)^{-1} \cdot \Delta a, \tag{8}$$

where Δa is the acceleration level. Similar to the pressure case, for high sensitivity, one would like $A_s Y_s / l_s \ll k_f$, which gives

$$\Delta T = \frac{\Delta T}{\Delta X} \cdot m_p k_f^{-1} \cdot \Delta a. \tag{9}$$

For a magnetic or electric field sensor, the constant C is $A_s Y_s d_{33}^{H,E}$, where $d_{33}^{H,E}$ is the magnetostrictive strain coefficient of the spacer material in the case of a magnetic field H_F or the piezoelectric strain constant in the case of an electric field E_F.

Accordingly, Eq. (3) becomes

$$\Delta T = \frac{\Delta T}{\Delta X} A_s Y_s d_{33}^{E,H} \left(k_f + \frac{A_s Y_s}{l_s} \right)^{-1} \Delta H_F, E_F. \tag{10}$$

As in the temperature case, Eq. (10) implies that for sensitive electric or magnetic field sensors $k_f l_s \ll A_s Y_s$, which yields

$$\Delta T \simeq \frac{\Delta T}{\Delta X} d_{33}^{H,E} l_s \Delta H_F, E_F. \tag{11}$$

For convenience, we repeat these simple equations together:

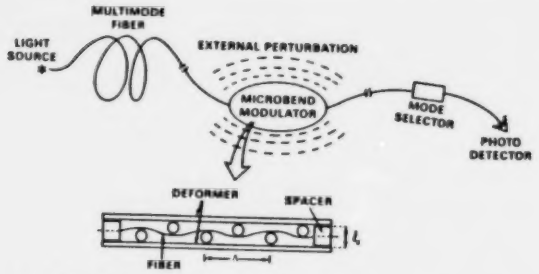

Fig. 1. Microbend fiber-optic sensor. Inset: sensing fiber with deformer.

$$\Delta T = \frac{\Delta T}{\Delta X} A_p k_f^{-1} \Delta P \quad \text{pressure,} \tag{5}$$

$$\Delta T = \frac{\Delta T}{\Delta X} \alpha_s l_s \Delta \theta \quad \text{temperature,} \tag{7}$$

$$\Delta T = \frac{\Delta T}{\Delta X} m_p k_f^{-1} \Delta a \quad \text{acceleration,} \tag{9}$$

$$\Delta T = \frac{\Delta T}{\Delta X} d_{33}^{H,E} l_s \Delta H_F, E_F \text{ magnetic/electric field.} \tag{11}$$

Equations (5), (7), (9) and (11) can all be written in the form of Eq. (1), where ΔE represents the environmental change, e.g., pressure and temperature, and D is a constant identified in the above equations for the various environmental sensors.

Under an environmental perturbation ΔE, the photodetector signal output i_s is given as[5]

$$i_s = \frac{q e W_0}{h \nu} \left(\frac{\Delta T}{\Delta X} \right) D \Delta E, \tag{12}$$

where h is Planck's constant, ν is the optical frequency, q is the detector quantum efficiency, e is the electron charge, and W_0 is the input optical power. Assuming a shot-noise-limited detection system, the mean square photodetector noise is given as[6]

$$i_N^2 = 2e(q e W_0 T / h\nu) \Delta f, \tag{13}$$

where Δf is the detection bandwidth. The S/N power ratio is thus

$$i_s^2 / i_N^2 = \left(\frac{q W_0}{h \nu} \right) \left(\frac{\Delta T}{\Delta X} \right)^2 D^2 (\Delta E)^2 (2T \Delta f)^{-1}. \tag{14}$$

The smallest signal that can be detected is given for the condition S/N = 1, which yields

$$\Delta E_{\min} = D^{-1} \left(\frac{\Delta T}{\Delta X} \right)^{-1} \sqrt{\frac{2Th\nu \Delta f}{q W_0}}. \tag{15}$$

The first factor is specific to the particular design of the environmental sensor; the second two factors, however, are general and apply to all environmental microbend sensors. We can define a generic microbend sensor as one which measures ΔX as defined by Eq. (2). Then from Eqs. (2) and (15) we have

$$\Delta X_{\min} = \left(\frac{\Delta T}{\Delta X} \right)^{-1} \sqrt{\frac{2Th\nu \Delta f}{q W_0}}. \tag{16}$$

If we know the performance of our generic sensor, we can predict the response of our specific sensor by sepa-

rately determining D. In what follows, we treat the generic microbend sensor. We consider optimization of the various components of this generic sensor including optical source, optical signal transmission fibers, and sensing fiber (both optical and mechanical issues). We have constructed an optimized version of the generic sensor and discuss its measured performance. Finally, based on these results and the expressions determined for D in this section, we determine the minimum detectable environmental changes ΔE for reasonable versions of the deformer.

III. Sensor Optimization

A. Sensing Fiber

1. *Periodicity*

For optimum sensor performance, the microbending sensitivity, $\Delta T/\Delta X$, of the sensing fiber must be maximized. One of the most important parameters in determining $\Delta T/\Delta X$ is the periodicity of the fiber deformation. To understand this dependence, let us briefly consider the mode coupling effect in fibers.

From the theory of mode coupling[7-10] it is well known that when a periodic microbend is induced along the fiber axis, light power is coupled between modes with longitudinal propagation constants k and k' satisfying[9,11]

$$k - k' = \pm \frac{2\pi}{\Lambda}, \tag{17}$$

where Λ is the mechanical wavelength of the periodic perturbation. Let us consider a fiber with refractive-index profile[12]:

$$n^2(r) = n^2(0)[1 - 2\Delta(r/a)^\alpha], \tag{18}$$

where $\Delta = [n^2(0) - n^2(a)]/2n^2(0)$. Here $n(0)$, $n(r)$, and $n(a)$ are the refractive indices at distances 0, r, and a from the fiber axis, respectively, a is the core radius, and α is a constant. A step profile corresponds to $\alpha = \infty$. Applying the WKB approximation[13] to the solution of the dielectric waveguide problem,[12,13] it can be shown that the wavenumber separation of neighboring modes is given for the profile of Eq. (18) by[14]

$$k_{m+1} - k_m = \frac{\alpha}{\alpha + 2} \frac{2\sqrt{\Delta}}{a} \left(\frac{m}{M}\right)^{[(\alpha-2)/(\alpha+2)]}, \tag{19}$$

where m is the modal group label and M is the number of modal groups.

For step-index fibers, Eq. (19) becomes

$$k_{m+1} - k_m = \frac{2\Delta^{1/2}}{a} \frac{m}{M}. \tag{20}$$

This means that the separation of modes in k space depends on the order of the modal groups m. From Eqs. (19) and (20) we see that high order modes (large m) can be coupled with small periodicity Λ, whereas low order modes (low m) are coupled with large Λ. The highest order core modes are coupled to radiated modes with periodicities obtained from Eqs. (17) and (20) with $m = M$:

$$\Lambda_c = \frac{\pi a}{\Delta^{1/2}} = \frac{\sqrt{2}\pi a n_0}{\text{N.A.}}, \tag{21}$$

where n_0 is the refractive index of the core and N.A. is the numerical aperture of the fiber. For parabolic-index fibers ($\alpha = 2$), Eq. (19) gives

$$K_{m+1} - K_m = \frac{(2\Delta)^{1/2}}{a}. \tag{22}$$

This means that in a parabolic-index fiber all modal groups are equally spaced in k space (to within the WKB approximation). In this case the same bending periodicity couples all adjacent modal groups. This critical mechanical periodicity Λ_c is given by

$$\Lambda_c = \frac{\sqrt{2}\pi a}{\Delta^{1/2}} = \frac{2\pi a n_0}{\text{N.A.}}. \tag{23}$$

In this paper, microbending loss is considered to be caused by coupling of guided to radiated modes. For small changes in the fiber deformation where neighboring mode coupling is believed to be valid, only adjacent modes are coupled. In this case, microbending loss is due to coupling of the highest guided mode to the first radiated mode. Such coupling can be realized with periodicities given by Eqs. (21) and (23) for step and graded fibers, respectively. Such periodicities are expected to enhance significantly microbending loss.

To verify the existence of the critical periodicities predicted by Eqs. (21) and (23), the microbending sensitivity was studied experimentally in a large number of optical fibers with step- and graded-index profiles as a function of periodicity Λ. Due to difficulty in accurately aligning the two plates of the deformer in measuring $\Delta T/\Delta X$, it was more convenient first to obtain $\Delta T/\Delta F$. A 5-cm fiber section was sandwiched between two circular plates with parallel corrugations, and force was applied to one of these plates. The periodicity was varied by rotating the fiber against the plates and using plates with different periodicities. An example of such an experiment is shown in Fig. 2 where $\Delta T/\Delta F$ is plotted vs periodicity at a bias force of $0.1N$ for a graded-index fiber made by Sumitomo. The fiber had a 0.13 N.A. and consisted of a 95-μm o.d. core, a 125-μm o.d. cladding, and a 135-μm o.d. UV curable coating. Special care was made to clamp firmly the ends of the bent fiber to avoid fiber sag.

The applied force ΔF, and the result in displacement ΔX are related by k_f, i.e., $k_f \Delta X = \Delta F$. Considering the bent fiber as a bar loaded at the center and clamped at its ends we have for k_f (Ref. 15)

$$k_f^{-1} = \frac{\Lambda^3}{3\pi Y d^4 \eta}, \tag{24}$$

where d is the diameter of the fiber, Y is the effective Young's modulus of the fiber, and η is the number of the bent intervals. Equation (24) was verified experimentally by monitoring the applied force ΔF and the resulted displacement ΔX in the $\Delta T/\Delta F$ vs Λ experiment. The relative displacement of one plate against the other was determined by observing the light fringes formed by a direct light beam and a beam reflected by a

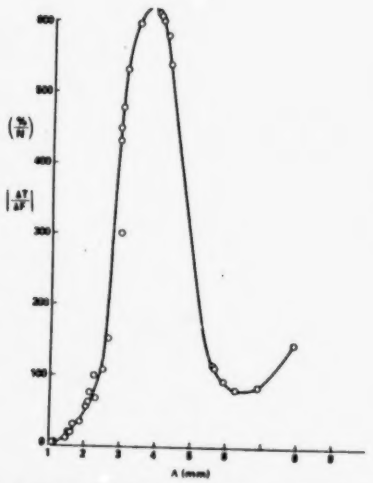

Fig. 2. Experimentally obtained $\Delta T/\Delta F$ vs periodicity (circles) for the Sumitomo graded-index fiber. Solid line: eye fit.

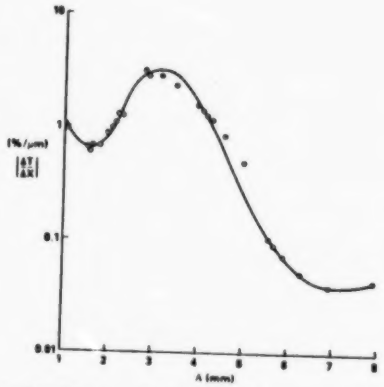

Fig. 3. Microbending sensitivity $\Delta T/\Delta X$ vs periodicity (circles) for the Sumitomo fiber. Solid line: eye fit.

mirror mounted to the movable plate. Equation (24) is valid for hard coatings only since soft coatings are deformed without communicating all the applied force to the glass fiber.

From Fig. 2 and Eq. (24), $\Delta T/\Delta X$ is obtained and is shown in Fig. 3 as a function of Λ for a force of $0.1N$. As can be seen from this figure, the microbending sensitivity exhibits a rather broad peak with its maximum at ~3 mm. This is in agreement with the prediction of $\Lambda_c = 3.35$ mm of Eq. (23) with $a = 47.5\ \mu$m and $\Delta = 0.004$ (N.A. = 0.13, $n_0 = 1.458$). Table I summarizes the experimental results obtained from several fibers with step- and graded-index profiles. As can be seen from this table, for graded fibers the analytically obtained [using Eq. (23)] critical periodicity is in good agreement with that found experimentally. For step fibers, the periodicity which couples the highest order core modes to radiated modes [Eq. (21)] is listed in Table I and agrees well with the experimentally found periodicity at which $\Delta T/\Delta X$ is maximum. The slightly lower value of the calculated Λ_c indicates that the fibers were partly graded. It can also be seen from Table I that fibers with a low N.A. and high core size have long Λ_c [Eqs. (21) and (23)]. This in turn results in more compliant fibers at Λ_c [Eq. (24)]. This enhances the sensitivity $\Delta T/\Delta F$ (Table I). On the other hand, fibers with small core size and high N.A., such as the Corning communications fiber (N.A. = 0.2, $a = 25\ \mu$m), have short Λ_c and very small sensitivity $\Delta T/\Delta F$.

2. *Length Dependence*

In designing the sensor, the length of the sensing fiber is an important parameter which influences both the bandwidth and sensitivity of the sensor. In the optimum case, the microbending sensitivity is expected to depend linearly on the length of the sensing fiber. It was found, however, that

$$\frac{\Delta T}{\Delta X} \propto l^q;\ 0 < q \leq 1. \tag{25}$$

To determine q, the induced loss ΔT_{loss} was monitored as a function of the applied force ΔF on different

Table I. Microbending Sensitivity of Fibers

Manufacturer	Profile	N.A.	Core radius (μm)	Clad radius (μm)	Analysis Λ_c (mm)	Exp. Λ_c (mm)	$\Delta T/\Delta F$ at Λ_c (% T/N)	$\Delta T/\Delta X$ at Λ_c (% T/μm)	Bias (N)
Hughes Research Laboratory	Step	0.133	30	62.5	1.46	1.5 ± 0.1	22	3.2	0.5
Sumitomo	Step	0.133	47.5	62.5	2.31	2.75 ± 0.3	180	1.5	0
Hughes Research Lab.	Step	0.14	31	90.0	1.43	1.7 ± 0.1	227	3.4	0.2
Times	Step	0.14	52.5	70.0	2.43	2.5 ± 0.2	240	2.0	0.2
EOTec	Step	0.05	44	62.5	5.70	6.0 ± 0.5	480	0.4	0.05
EOTec	Step	0.125	42.5	85.0	2.20	2.5 ± 0.2	70	1.7	0.6
EOTec	Step	0.11	50	67.5	2.95	3.1 ± 0.2	95	2.0	0.4
EOTec	Step	0.1	76	104	4.92	5.0 ± 0.5	100	0.7	0.2
Times	Graded	0.132	26	66.0	1.80	1.8 ± 0.05	170	3.8	0.4
Corning	Graded	0.168	50	62.0	2.73	2.7 ± 0.1	210	2.0	0.2
Times	Graded	0.143	100	125	6.41	6.0 ± 0.2	50	0.7	0.6
Corning	Graded	0.2	26	62.5	1.15	1.14 ± 0.1	13	2.0	0.25
Sumitomo	Graded	0.13	47.5	62.5	3.35	3.2 ± 0.3	620	3.2	0.1
Sumitomo	Graded	0.166	47.5	62.0	2.62	2.8 ± 0.2	280	2.0	0.1
Sumitomo	Graded	0.144	48.2	61.5	3.17	2.9 ± 0.2	120	0.7	0

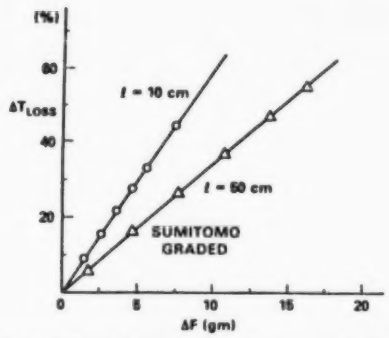

Fig. 4. Microbending induced loss ΔT_{loss} vs applied force ΔF for two lengths of deformed Sumitomo fiber. Solid lines: best linear fits to data.

lengths l of the fiber bent at Λ_c. The results of such an experiment are shown in Fig. 4 for 10- and 50-cm length of bent fiber. The fiber was the Sumitomo 0.13 N.A. UV curable coated graded-index fiber. From the slope of the best linear fit to the data q was determined. The results of these experiments are summarized in Table II. The value of q is small for coatings such as silicone which allow recoupling of the clad modes back to core modes. With highly absorbing coatings, however, such coupling is prevented, and values of q close to 1 are obtained.

In reference to Fig. 4, it should also be noticed that the linear relationship between ΔT_{loss} and ΔF demonstrates that the microbending sensitivity is constant over a wide range of applied force. This linearity, which can be achieved only with all core modes equally excited, indicates that the dynamic range of the sensor is large.

3. *Macrobending Loss Effect in Multimode Fibers*

In designing the microbend sensor it is important to consider the macrobending effect, i.e., light power loss caused by fiber deformations of the order of centimeters. Even though such macrobends cannot introduce mode coupling [which requires small bends; Eqs. (20) and (22)], they extend the field of the propagating modes into the coating,[16] which in turn can introduce losses. In particular, macrobending removes the preferred higher order core modes, which, as we have seen before, provide the microbending sensitivity. Therefore, macrobending can significantly decrease the microbending effect and must be avoided.

The macrobending effect was studied experimentally in both step- and graded-index fibers. Figure 5 shows macrobending loss vs bend diameter for the

Table II. Length Dependence of $\Delta T/\Delta X$

$\Delta T/\Delta X \sim l^q$	
Coating	q
Silicone	0.2
UV elastomer	0.6
Aluminum	0.7
Black paint	1.0

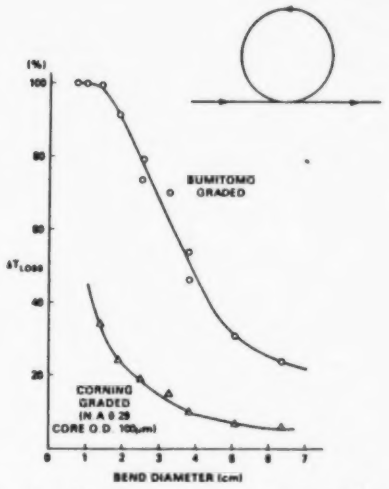

Fig. 5. Macrobending induced loss ΔT_{loss} vs bend diameter for the Sumitomo fiber and a Corning graded fiber. Solid lines: eye fits.

Sumitomo-graded fiber of 0.13 N.A. The fiber was bent with one loop, the coating was removed, and the glass fiber was painted with a highly absorbing oil paint. As can be seen from Fig. 5, bends of the order of 2 cm in diameter or smaller remove most of the guided light. For comparison, in Fig. 5 is also shown macrobending losses of a standard Corning graded fiber of 0.29 N.A. In this fiber, macrobending losses are high for bends of <1.5-cm diameter. As can be seen from Figs. 2 and 5, fibers with high microbending sensitivity are expected to have enhanced macrobending losses.

Tables III and IV summarize the experimentally obtained macrobending sensitivity as a function of bent diameter for several step and graded fibers, respectively, with both their coatings on and replaced with a highly absorbing paint. For fibers with low absorbing coatings, such as silicone, macrobending losses increased significantly when the absorbing paint was used. In general, macrobending losses are high in low N.A. fibers for bends of less than ~4-cm o.d. Graded fibers appear to have relatively higher macrobending losses than step fibers (Table III vs Table IV).

B. Light Source

It is well known[17,18] that coherent light from a laser propagating in a multimode fiber introduces significant speckle caused by interference of various guided modes. This speckle is very sensitive to the optical fiber lead environment (described below), causing significant lead noise and sensor instability. On the other hand, an incoherent light source, such as a LED, minimizes speckle and lead noise increasing the sensor stability.

In addition to the speckle problem, the intrinsic noise of a laser diode is higher than that of a LED. This can be seen from Figs. 6 and 7 where the sensor noise is shown with (upper trace) and without (lower trace) the light source. In Fig. 6 an Optical Information Systems OL5000 DI-Pa laser diode (light power:

Table III. Macrobending Sensitivity of Step Fibers

	P44 Hughes	P115 Hughes	S-20 Times	EOTec EPC-BC600	EOTec 13151		EOTec 11751		Valtec		NSG 51-100H		NSG 51-100A		Times 100449A		Sumitomo
Core o.d. (μm)	60	62	105	95	88		85		200		100		100		200		95
Clad o.d. (μm)	125	180	140	135	125		170		Plastic		150		150		250		125
N.A.	0.133	0.14	0.14	0.11–0.12	0.05		0.125		0.3		0.5		0.267		0.172		0.133
Bend diam (cm)	Coat	Coat	Coat	Bare	Coat	Coat	Bare	Coat	Bare	Coat	Coat	Bare	Coat	Bare	Coat	Bare	Coat
							ΔT_{loss} (%)										
0.96	19.0	59.5		84.6	9.6	29		17.8						25.3	7.78		
1.11	15.9	54.9	11.0	83.4	21.1	28		17.8					0.37	20.6	5.49		
1.37	7.9	43.9	8.9	80.3	7.9	37		16.6			1.48		0.19	14.7	3.32		
1.92	4.8	28.6	5.9	71.6	7.9	33		13.4		6.3	1.33	0.09	0.14	12.6	4.19		
2.12	3.6	21.4	7.5	68.6	7.1	45		11.5		6.3	1.18	0.05	0.10	10.3	2.2		
2.53	3.0	15.0	6.7	64.7	5.4	42		8.3		6.3	1.18	0.05	0.09		1.6		76
3.30	2.2	9.9	6.1	51.6	4.4	34		7.1	48.7		1.17	0.05	0.03	6.26	2.7		68
3.83	2.5	7.6	4.4	34.2	3.2	40	100	4.5	30.4	0	0.58	0.05	0.05	2.72	0.55		63
5.10	1.6	6.1	4.2	17.9	2.0	24	99.5	1.9	8.8	0	0.86	0.05	0.04	4.08	0.56		34
6.34	1.8	3.8	4.7	11.7	1.4	21	90.8	1.3	8.5	0	0.57	0	0.03	2.26	0.56	5.1	

720 μW) was used, and in Fig. 7 a Fujitsu FED081SA LED (light power: 725 μW) was used. As can be seen from these figures, an excess noise of ~20 dB was introduced by the laser diode, while the LED was found to be shot-noise-limited. Similar performances were obtained from several laser diodes and LEDs. Superluminescent diodes were also studied and found to have intermediate performance. Only a truly incoherent light source, such as a LED, avoids the speckle problem. The elimination of speckle and the low intrinsic noise demonstrate the superior performance of LEDs over laser diodes when they are used as light sources in intensity sensors utilizing multimode fibers. This difference is more dramatic at low frequencies where laser noise is inversely proportional to frequency, while a LED remains almost shot-noise-limited to very low frequencies.

C. Fiber Sensor Leads

To minimize noise, the sensor should be insensitive to the lead environment. As mentioned above, an incoherent light source, such as a LED, minimizes speckle and thus lead noise. However, any intensity modulation in the band of operation introduced by the fiber leads, which can be very long and located in a hostile environment, will generate excess noise degrading the sensor performance. The excess noise is primarily introduced by power modulation in the highest order guided modes caused by either microbending (mode coupling to the radiated modes) or macrobending. On the other hand, the light power in the lower order guided modes is expected to be more stable since any power loss to other modes will be partly compensated by a power gain from other modes. Thus, by rejecting the high order modes, any power modulation introduced by the fiber leads will be minimized. This rejection can be done very easily by using as leads standard fibers made for communications application with a much higher N.A. than that of the sensing fiber, which should have a relatively low N.A. for high microbending sensitivity. The core sizes of the lead and sensing fibers should be the same for minimizing fusion losses. At the fusion where light is coupled from the high N.A. lead fiber to the low N.A. sensing fiber, all light from the high order modes is rejected automatically together with any lead noise. At the second fusion, light from the low N.A. sensing fiber is coupled only to the low order modes of the second high N.A. lead fiber. Thus any modulation of the total light power propagated in this fiber is also minimized.

D. Detection

Any environmental change can be detected by monitoring the light power in certain group of modes which are separated by the mode selector (Fig. 1) and then detected. In this paper, microbending loss is due to the total light power change in all core modes. In this case, all the core modes are detected (light field) by using as mode selector an absorbing coating which removes any light from the clad modes. The high background of the light field limits the detectability of

Table IV. Macrobending Sensitivity of Graded Fibers

	Corning Standard		Corning 515301		Corning exp.		Times 100377C		Valtec 21674		Sumitomo 2	Sumitomo 3	Sumitomo 4
Core o.d. (μm)	50		63 × 73		100		52		100		96.3	95	
Clad o.d. (μm)	125		135 × 138		124		132				123	125	
N.A.	0.20		0.16		0.168		0.132		0.21		0.144	0.13	
Bend diam (cm)	Coat	Bare	Coat	Bare	Coat	Bare	Coat	Bare	Coat	Bare	Coat	Coat	Coat
	ΔT_{loss}												
0.96	51.1		47.8		87		30.3	95.7	62.8		82	100	
1.11	46.7		43.0	40.9	81		25.6	89.7	53.6	59.4	78	100	
1.37	40.6		34.5	33.6	76		25.3	78.4	46.1	47.1	75	99.4	
1.92	27.8	26.9	24.7	21.9	57	53.1	19.3	58.3	30.7	32.2	60	91.5	
2.12	23.3	25.1	21.8	20.3	54	50.0	21.2	52.3	23.7	27.3			
2.53	18.9	19.3	16.2	15.2	45	39.9	13.7	44.9	22.8	24.9	44	78.8	41.1
3.30	17.6	14.8	11.3	11.6	34	29.6	13.4	44.4	16.6	18.2	27	69.9	34.2
3.83	13.2	11.2	9.2	8.63	21	21.6	9.6	26.6	12.1	13.3	13	45.4	20.7
5.10	9.9	8.2	6.3	5.80	16	15.1	5.1	24.7	7.6	9.94	7.5	30.5	12.7
6.34	5.5	5.9	4.2	4.35	13	6.67	3.6	10.1	6.7	3.89	4.3	23.4	8.25

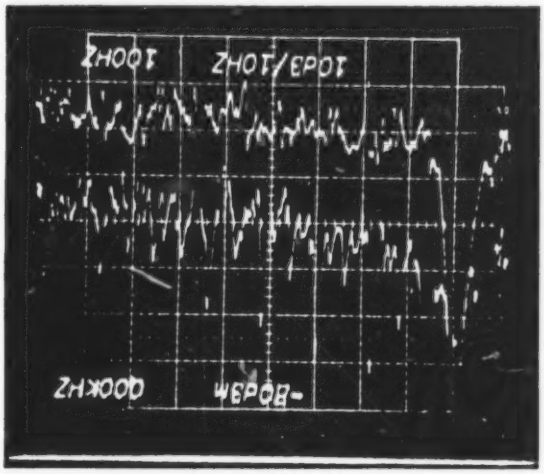

Fig. 6. Sensor noise with (upper trace) the light source (laser diode: Optical Information Systems OLS000; light power, 720 μm) and without (lower trace) the light source.

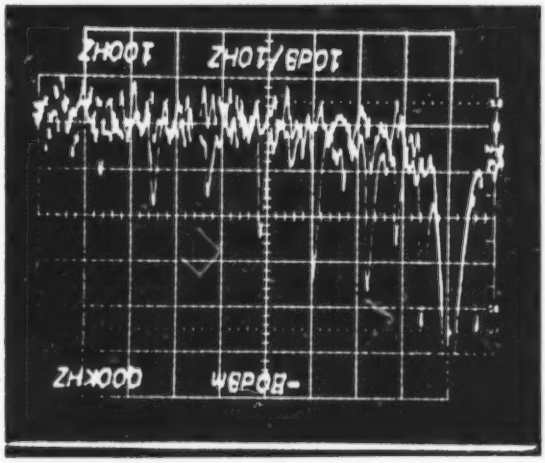

Fig. 7. Sensor noise with (upper trace) the light source (Fujitsu FED081SA LED; light power, 725 μm) and without (lower trace) the light source.

the sensor. However, high sensitivity can be achieved by utilizing long lengths of sensing fiber with an absorbing coating [Eq. (25)]. In this detection, an inexpensive PIN diode is an appropriate detector to be used.

Although not used here, the light power in the clad modes can also be detected (dark field). Selection of the clad modes can be done immediately after the deformer by using, e.g., a sphere detector filled with a stripping liquid[4,19] or a clad-to-core coupler, which couples the clad modes of the sensing fiber-to-core modes of the lead fibers. Such a coupler can be made using the biconical method[20] by appropriately twisting, heating, and nonuniformly stretching the two fibers. Using such a coupler, the clad modes in the sensing fiber become core modes in the lead fiber which can then be conveniently detected. In the dark-field detection, any light coupled to the clad modes of the sensing fiber introduces a significant modulation in the small background of the clad modes which they can be easily stripped just before the deformer. The small background is introduced by the bias applied on the sensing fiber for dynamic range considerations. As can be seen from Fig. 4, however, this bias can be kept minimum without deteriorating the microbending sensitivity of the sensing fiber. Therefore, the dark field can minimize noise providing good detectability for short sensors having a small stable bias. Long lengths of sensing fiber, however, while providing high sensitivity, increase the light background in the clad modes and thus eliminate the dark-field benefits.

With the core and clad modes separately selected, a differential detection scheme can be utilized. Similar detection is also possible when high and low core modes are separately selected. Such a differential detection is expected to decrease noise improving the sensor detectability.

IV. Generic Microbend Sensor Performance

The generic microbend sensor described in this section is based on microbend-induced losses due to cou-

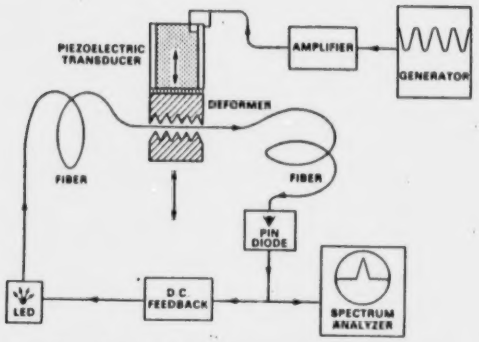

Fig. 8. Generic microbend (displacement) fiber-optic sensor.

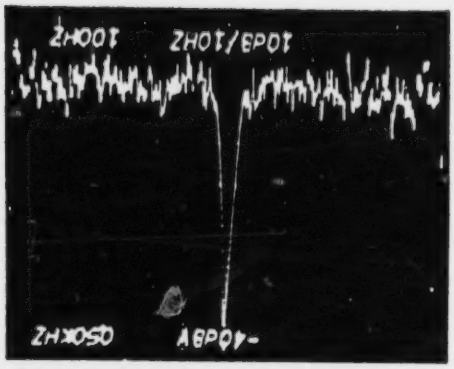

Fig. 9. Spectrum obtained experimentally from the microbend displacement sensor. Signal at 1 kHz. Bandwidth, 10 Hz. Driving displacement: 10 Å.

pling of core-to-clad modes, and it is shown schematically in Fig. 8. The sensing fiber was the Sumitomo 0.13 N.A. graded fiber. The deformer consisted of two corrugated plates of Lucite with fourteen teeth, each having a 3.35-mm periodicity, which is the critical periodicity of the sensing fiber (Figs. 2 and 3). The sensing fiber was kept straight to avoid macrobending losses.

To eliminate speckle and operate as close to the shot noise limit as possible, a LED was utilized as the light source. The signal, i.e., the modulation of the light in all core modes, was detected by a PIN diode whose output was read by a spectrum analyzer. The lead noise was significantly minimized by using as leads a high N.A. (0.29, Corning graded) fiber. The core diameter (100 μm) of the lead fiber was similar to that (95 μm) of the sensing fiber for minimizing fusion losses.

One plate of the deformer could be displaced relative to the other by manually adjusting a micrometer, while the other plate could be displaced electrically by a piezoelectric transducer. The piezoelectric transducer was calibrated using an accelerometer. From this calibration (24 Å/V) and the signal, the dynamic sensitivity of the sensor $\Delta T/\Delta X$ was found to be 0.45 μV/Å (which is equivalent to a 24% change of light power per 1-μm change in the fiber deformation). This sensitivity was found to be in agreement with the static sensitivity (using the micrometer). By varying the applied voltage on the piezoelectric transducer, the dynamic range of the sensor was found to be ~140 dB.

Figure 9 shows a typical spectrum obtained experimentally with a 10-Å driving displacement at 1 kHz (detection bandwidth: 10 Hz). In this case, the SNR is 58 dB. The minimum detectable displacement was then calculated from the SNR in the frequency range of 100–1000 Hz. It was found to be ~0.01 Å, in agreement with that predicted from Eq. (16) for a shot-noise-limited system. This detectability is ~2 orders of magnitude better than that reported previously.[4] In that sensor, the limited SNR is due (a) to the low sensitivity of the sensing fiber which was not optimized to microbending losses and (b) to excess noise introduced by the laser used (125 Spectra-Physics He–Ne laser with an ~20-dB higher noise than a shot-noise-limited LED).

To assess the stability of the sensor, the fiber leads were subject to strong mechanical vibration. No signals were observed even at the frequency of the perturbation or did these affect the sensitivity of the sensor itself.

V. Predicted Environmental Performance

For each environmental sensor, we can now estimate the minimum detectable changes in the measured quantities. Specifically, Eqs. (16) and (15) can be combined to give

$$\Delta E_{min} = D^{-1}\Delta X_{min}, \tag{26}$$

with ΔX_{min} now equal to 0.01 Å.

A. Pressure Sensor

From Sec. I, $D = A_p k_f^{-1}$. Equation (26) becomes

$$\Delta P_{min} = \frac{\Delta X_{min}}{A_p k_f^{-1}}. \tag{27}$$

Therefore, high detectability (small ΔP_{min}) can be achieved with high k_f^{-1}. This can be obtained with large Λ [Eq. (24)], which for high $\Delta T/\Delta X$ should be Λ_c. High Λ_c requires fibers of low N.A. [Eqs. (21) and (23)]. This can be also seen from Table I where the lower N.A. fibers have higher $\Delta T/\Delta F$. For example, the 0.133 N.A. fiber shown in Fig. 2 has 50 times higher $\Delta T/\Delta F$ than the 0.2-N.A. Corning communications fiber, even though both fibers were graded of the same outer diameter (125 μm). However, the low N.A. limit is determined by the light source rather than $\Delta T/\Delta F$, since in general the light power coupled into the fiber is proportional to (N.A.)^2. In addition to low N.A., high Λ_c can be obtained with large core size [Eqs. (21) and (23)]. However, for pressure sensors where k_f^{-1} is the controlling factor [Eq. (4)], it is the core-to-clad ratio (to the third power) which should be maximized to increase k_f^{-1} [Eq. (24)]. This can be verified from Table I. Also, fibers with smaller Young's modulus and/or smaller outer diameter will increase k_f^{-1} [Eq. (24)]. Finally, k_f^{-1} is inversely proportional to the number of fiber deformations n. As can be seen from Table II, however, for fibers with absorbing coatings

$\Delta T/\Delta X$ is proportional to n, and thus ΔX_{min} becomes independent of n.

For $A_p = 1$ cm^2 and $k_f^{-1} = 33 \times 10^{-8}$/dyn/cm (for the fiber shown in Figs. 2 and 3) we obtain $\Delta P_{min} = n \cdot 3 \times 10^{-4}$ dyn/cm^2. For a static pressure sensor, this represents a very sensitive device. As a dynamic pressure sensor (microphone), this level is comparable with that achievable by the human ear at ~1 kHz. If the deformer is 1 mm thick and made from aluminum, the first mechanical resonance would be in the neighborhood of 4 kHz, so that the response would be approximately independent of frequency to several kilohertz. As a hydrophone, the above minimum detectable pressure is comparable to the best available devices made from piezoelectric technology. However, special mounting designs would have to be employed to deal with static pressure caused by operation at significant depths.

B. Temperature Sensor

From Sec. II, $D = \alpha_s l_s$. Taking the deformer supports to be 1 cm long and made from aluminum ($\alpha_s = 24 \times 10^{-6}$/°C), we find $\Delta\theta_{min} = 4 \times 10^{-6}$°C, which is an exceptional sensitivity.

C. Acceleration

From Sec. II, $D = m_p k_f^{-1}$. Taking the plates to be 1 cm^2 and a 1-mm thick piece of lead, m_p is 1 g. With $k_f^{-1} = 33 \times 10^{-8}$/dyn/cm we obtain $a_{min} = n \cdot 3 \times 10^{-7}$ g. This is competitive with the best conventional accelerometers.[21] The first resonant frequency would be ~2 kHz.

D. Magnetic Field Sensor

From Sec. II, $D = d_{33}^H l_s$. Using magnetostrictive Permalloy deformer supports 1 cm long ($d_{33}^H = 10.4 \times 10^{-7}$/G), we find $\Delta H_{min} = 9.6 \times 10^{-5}$ Oe. This is only a moderate detectability which can be provided by low cost (~$2000) commercially available magnetic sensors used for applications such as inspection, production testing, and magnetic locators.[22] Compared to comparable predictions for a 10-cm interferometric fiber-optic magnetometers,[1] this level is ~3 orders of magnitude lower.

E. Electric Field Sensor

From Sec. II, $D = d_{33}^E l_s$. Using piezoceramic (PZT-5H) deformer supports 1 cm long ($d_{33}^E = 593 \times 10^{-12}$ m/V) we find $\Delta E_{min} = 1.7 \times 10^{-1}$ V/m. This detectability is significantly lower than that provided by a good antenna.

VI. Summary

The microbending effect has been considered in multimode fibers as a transduction mechanism for sensing environmental changes, such as pressure, temperature, acceleration, and magnetic and electric fields. By studying a generic design, the microbend sensor has been examined and optimized. First, the microbending sensitivity of multimode fibers has been studied and found to increase dramatically at certain deformation periodicities, in agreement with analytical predictions based on neighboring mode coupling. The microbending sensitivity was also found to depend linearly on the length of the bent fiber having highly absorbing coatings, while for fibers with less absorbing coatings the dependence is weaker. Then the macrobend effect was studied experimentally in several multimode fibers, and it was found that bends with a radius of <2 cm cause significant losses which can dramatically minimize microbending sensitivity.

In addition to the sensing fiber, the other components of the microbend sensor have been also considered. Various light sources were examined, and it was found that LEDs give much better performance, especially at low frequencies than lasers by minimizing speckle, which can introduce signficant lead noise and sensor noise. The sensor lead noise, which is minimum with LEDs, can be further reduced by using high N.A. lead fibers with relatively low N.A. sensing fibers. Such a combination automatically rejects any light from the high order modes which carry most of the lead noise. Then various detection schemes, which can be utilized in microbend sensors, were examined, and their advantages were discussed.

An optimized generic microbend sensor was built and utilized to detect displacement. The sensor was found to have good detectability (0.01 Å), wide dynamic range, and high stability to lead environment. Finally, based on this generic sensor performance, the predicted minimum detectable environmental changes in detecting pressure, temperature, acceleration, and magnetic and electric fields were found to be very promising for most cases.

References

1. T. G. Giallorenzi, J. A. Bucaro, A. Dandridge, G. H. Sigel, J. H. Cole, S. C. Rashleigh, and R. G. Priest, "Optical Fiber Sensor Technology," IEEE J. Quantum Electron. **QE-18**, 626 (1982).
2. J. A. Bucaro, N. Lagakos, J. H. Cole, and T. G. Giallorenzi, *Physical Acoustics, Vol. 16* (Academic, New York, 1982), p. 385.
3. N. Lagakos, W. J. Trott, T. R. Hickman, J. H. Cole, and J. A. Bucaro, "Microbend Fiber-Optic Sensor as Extended Hydrophone," IEEE J. Quantum Electron. **QE-18**, 1633 (1982).
4. N. Lagakos, T. Litovitz, P. Macedo, R. Mohr, and R. Meister, "Multimode Optical Fiber Displacement Sensor," Appl. Opt. **20**, 167 (1981).
5. J. N. Fields, C. P. Smith, C. K. Asawa, R. J. Morrison, O. G. Ramer, G. L. Tangonan, and M. K. Barnoski, "Multimode Optical-Fiber Loss- Modulation Acoustic Sensor," in *Technical Digest, Conference on Optical Fiber Communication* (Optical Society of America, Washington, DC, 1979), paper WD3; also J. N. Fields, C. K. Asawa, O. G. Ramer, and M. K. Barnoski, "Fiber Optic Pressure Sensor," J. Acoust. Soc. Am. **67**, 816 (1980).
6. A. Yariv, *Introduction to Optical Electronics* (Holt Rinehart & Winston, New York, 1971), p. 254.
7. D. Gloge, "Optical Power Flow in Multimode Fibers," Bell Syst. Tech. J. **51**, 1767 (1972).
8. D. Marcuse, *Theory of Dielectric Optical Waveguides* (Academic, New York, 1974).
9. D. B. Keck, *Fundamentals of Optical Fiber Communications*, M. Barnoski, Ed. (Academic, New York, 1976).
10. J. E. Widwinter, *Optical Fibers for Transmission* (Wiley, New York, 1979).

11. L. Jeunhomme and J. P. Pocholle, "Mode Coupling in a Multimode Optical Fiber with Microbends," Appl. Opt. **14**, 2400 (1975).
12. D. Gloge and E. A. J. Marcatili, "Multimode Theory of Graded-Core Fibers," Bell Syst. Tech. J. **52**, 1563 (1973).
13. E. Merzbacker, *Quantum Mechanics* (Wiley, New York, 1961).
14. C. N. Kurtz and W. Streifer, IEEE Trans. Microwave Theory Tech. **MTT-17**, 250 (1969).
15. F. L. Singer, *Strength of Materials* (Harper and Brothers, New York, 1962), p. 265.
16. E. A. J. Marcatili and S. E. Miller, "Improved Relations Describing Directional Control in Electromagnetic Wave Guidance," Bell Syst. Tech. J. **48**, 2161 (1969).
17. J. W. Goodman, "Fundamental Properties of Speckle," J. Opt. Soc. Am. **66**, 1145 (1976).
18. B. Crosignani, B. Daino, and P. DiPorto, Opt. Commun. **11**, 178 (1974).
19. A. R. Tynes, "Integrating Cube Scattering Detector," Appl. Opt. **9**, 2706 (1970).
20. B. S. Kawasaki and K. O. Hill, "Low-Loss Access Coupler for Multimode Optical Fiber Distribution Networks," Appl. Opt. **16**, 1794 (1977).
21. e.g., Wilcoxon Research, Bethesda, MD, Specification Sheet 1000.
22. e.g., Schonstedt Instrument, Reston, VA, General Catalog (1985).

Patents *continued from page 2163*

4,639,139 27 Jan. 1987 (Cl. 356–359)

Optical profiler using improved phase shifting interferometry.

J. C. WYANT and K. N. PRETTYJOHNS. Assigned to Wyko Corp. Filed 27 Sept. 1985.

This patent describes a general method of measuring phase information in interferometric systems. The method involves using a piezoelectric transducer to vibrate the reference mirror. The sinusoidal variation of the intensity at each point of the interferogram is then sampled at four time slots for calculation of the phase. This phase measurement technique was applied to a Mirau interferometer for measuring surface profile and a Mach-Zehnder interferometer for measuring the wavefront quality of collimated beams from laser diodes. W.-H.L.

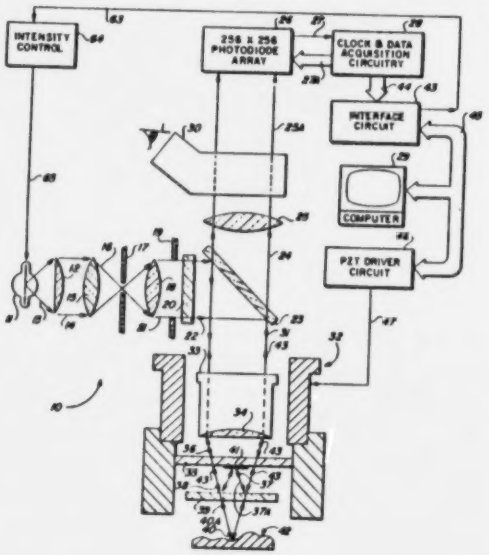

4,640,615 3 Feb. 1987 (Cl. 356–130)

Liquid refractometer.

I. SASAKI. Assigned to Issei Sasaki; Seiko Instruments & Electronics, Ltd. Filed 15 Oct. 1984.

A probe is directly dipped into a liquid whose refractive index is to be measured in real time. Two coherent light beams are linearly polarized at right angles and sent to sample and reference paths. A phase difference is detected between both beams. Previous refractometers either do not measure refractive index in real time or suffer from inaccuracies which are not smaller than ~1 part in 1000. This invention overcomes both limitations. One application is to monitor the production processes of optical fibers. A.B.

4,641,928 10 Feb. 1987 (Cl. 350–427)

Four-group telephoto zoom lens.

Y. HAMANISHI. Assigned to Nippon Kokagu K.K. Filed 27 Mar. 1984 (in Japan 30 Mar. 1983).

Six examples are given of a conventional four-component zoom lens having three elements in the front positive focusing unit, four elements in the negative variator, a cemented positive doublet for the compensator, and a four- or five-element rear relay unit. The six examples cover a wide range of focal lengths and apertures from 70–210 mm at f/4 up to 200–600 mm at f/9.5. The designs are controlled by five conditions, and excellent aberration correction is claimed. R.K.

4,641,929 10 Feb. 1987 (Cl. 350–432)

Biaspherical lens.

J. J. M. BRAAT. Assigned to U.S. Philips Corp. Filed 7 Jan. 1985 (in the Netherlands 22 Oct. 1984).

A single biaspheric lens element for use in a videodisc recorder is constructed from a sphere of glass or quartz with molded plastic aspherical surfaces formed on opposite sides of the sphere. Glass spheres can be generated cheaply by well-known methods. The base sphere may have a diameter of the order of 5 mm, the resulting biaspheric lens having a numerical aperture of 0.45, covering a field ~150 μm in diameter. R.K.

4,641,934 10 Feb. 1987 (Cl. 351–159)

Ophthalmic lens with diffractive power.

M. H. FREEMAN. Assigned to Pilkington P.E., Ltd. Filed 20 Sept. 1983 (in U.K. 29 Sept. 1982). Continuation-in-part of Ser. 368,362, 14 Apr. 1982).

This invention is based on an assumption that the chromatic aberration of the human eye reduces the amount of accommodation required to view objects over a range of distances. An increase of chromatic aberration is to be effected by adding a hologram having a large chromatic aberration (diffractive power) to an auxiliary lens of low aberration placed before the eye. Information on producing this hologram is given only by reference to another patent application (Serial 368,362). Adequate disclosure for practice of this invention by this patent seems doubtful. J.J.J.S.

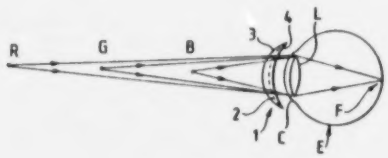

4,642,113 10 Feb. 1987 (Cl. 623–6)

Intraocular lenses.

S. DUBROFF. Filed 8 July 1985. Continuation of 496,529, 23 May 1983, abandoned; 230,279, 30 Jan. 1981, abandoned.

The claims of this invention are primarily directed to configurations of curved plastic positioning members devised to support and locate a transparent lens implant in the anterior chamber of the eye. This implant replaces the original lens which has been removed because of a cataract condition. The shape of these plastic supports is claimed to avoid irritation of the cornea and iris and prevent the lens from pupillary capture. J.J.J.S.

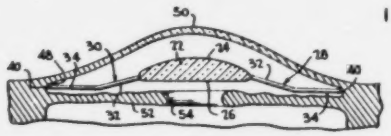

4,643,536 17 Feb. 1987 (Cl. 350–422)

Rear conversion lens.

Y. YAMADA, Y. SATO, H. NAKAYAMA, and K. OIZUMI. Assigned to Canon K.K. Filed 28 June 1985 (in Japan 2 July 1984).

A telenegative attachment lens is described consisting of an airspaced assembly of three elements (− + −), which can be mounted behind a main lens to increase its focal length and f/No. by a factor of 1.4 or 1.6. Three examples are given together with a particular f/2.8 Tessar objective, although a lens of some other type could be used. The design is controlled by seven conditions. R.K.

continued on page 2187

Wide range optical fibre microbending sensor

Kevin E. Lindsay and Barry E. Paton

Physics Department, Dalhousie University
Halifax, Nova Scotia, Canada B3H 3J5

Abstract

Several different coated fibres, representing both the step index and graded index groups, were tested for their sensitivity to bending using a mandrel wrap technique. Different sensor designs indicated that a grooved block arrangement was most suitable. A linear response over a large dynamic range was obtained by pretensioning the fibre in the sensor head.

Introduction

In the last decade there has been much effort in the development of fibre optic sensors[1,2,3] to measure a growing range of physical parameters, such as pressure, displacement, etc. This new generation of all-dielectric sensors is completely impervious to electromagnetic interference (EMI) and is thus particularly suited for use in electrically noisy environments such as those found in the modern industrial workplace.

Phase modulations in single mode fibre sensors have been used extensively in interferometric configurations[4,5] for optical gyroscopes, hydrophones, and magnetic field sensors. While phase modulation provides exceptional sensitivity and an elegant measurement technique, precision optical components make these sensors too costly for general industrial usage. On the other hand, intensity modulated sensors based on induced microbending losses[6] are attractive for two reasons. Firstly, the fibre used for communication with the sensors can itself become the sensor. Secondly, the availability of low cost fibres, sources, and detectors make these sensors cost effective.

In this paper, we present results on the development of a wide dynamic range microbending sensor using multi-mode optical fibres.

Microbending sensors

It is well known that the transmission losses of optic fibres will increase when the fibre is subjected to any form of mechanical distortion. In the case of microbending along the fibre axis, the guided light within the core couples into radiating modes and is subsequently lost. Light coupling between the guided modes, with propagation constant K, and the radiating modes, with propagation constant K°, is strongest when

$$K - K^{\circ} = \pm \frac{2\pi}{\Lambda} \qquad (1)$$

where Λ is the mechanical wavelength associated with a periodic perturbation[7]. In multi-mode fibres, with hundreds of modes, this relationship is easily satisfied and large losses occur.

Care must be taken to ensure the fibre is not distorted beyond its minimum bend radius where the fibre will break. Microcracks present on the fibre surface, when under bending forces, can grow into a macro-break causing a catastrophic failure of the sensor. This occurs when the fibre experiences high tensile forces as in the case of bending beyond the critical bend radius. Specially designed polymers extruded around the fibre at manufacture form a soft coating which not only protects the fibre against future nicking, but also serves to minimize microcrack growth by distributing any tensile forces along a bent fibre section.

In addition, the coating can provide a limited hermetic seal against contaminants in a hostile environment. One element which dramatically decreases the sensor lifetime is water. In marine applications a sensor must be sealed from accidental flooding.

In the simplest form of mechanical distortion, a fibre is wrapped around a mandrel. The loss curve, as a function of bend radius, quickly reveals the sensitivity of a fibre to bending. Most microbending sensors use periodic distortions produced by placing the fibre between corrugated plates. Many different jaw shapes have been used and all shapes produce satisfactory bending losses. Care must be taken, however, to ensure the distortions cycled over many times do not lead to fatigue and hence catastrophic failure. A novel approach by Marvin and Ives[8] uses a roller chain mechanism to impose a sinusoidal distortion along the fibre. We have observed that the corrugated shape is critical and have chosen a grooved D-structure (Fig. 1). This design ensures that the elastic limit of the fibre is not exceeded and the shape is self-limiting when the fibre fills the cavity.

The experimental apparatus used to investigate the microbending loss of coated fibres is shown in Figure 2. A Burr-Brown 3712T transmitter ($\lambda = 670$ nm) was used to illuminate the test fibre. A mode scrambler was used to distribute power amongst all guided modes and a stripper, formed by cementing a section of uncoated fibre into index matching glue,

removed the cladding modes. One of the deforming blocks was firmly mounted on an optical bench, while the other was attached to a translation stage and could be displaced relative to the first block by adjusting the stage's micrometer setting. During pretension experiments a pulley and mass arrangement was used to supply a controlled tension. The amount of light reaching the end of the fibre was detected using a Burr-Brown 3712R receiver. A computer-driven stepping motor allowed precision control of the block's motion throughout the operating displacement range from zero to 600 μm.

Microbending results

Six commercially available coated optical fibres, Table 1, were wrapped around a precision set of mandrels. The induced attenuation as a function of bend radius, Figure 3, is shown for a Corning Corguide 100/140 micron step index fibre. In the insert, a log-log plot of loss versus bend radius, shows the excellent fit of our results to the expression

$$LOSS = C/R^m \qquad (2)$$

where C is an experimental constant and the power m is related to the bend sensitivity. Most samples followed this simple power relationship. For the test set of samples, the Corning step index fibre displayed the highest sensitivity. This is a surprising result in that it is commonly expected that graded index fibres will be more sensitive to bending[9].

FIBRE	CORE/CLAD DIM (μm)	LOSS† (dB)	BREAKING RADIUS(mm)	SLOPE/ INTCPT
Corning Corguide (SI)	100/140	-7.2	0.9	-1.59/3.03
Cortland (SI)	100/140	-6.9	1.0	-1.41/3.02
Sieverts Ericsson (SI)	200/300	0.0*	1.5	*
Corning EN001 (GI)	100/140	-4.2	0.8	-1.36/2.43
Corning EN002 (GI)	100/140	-4.0	0.8	-1.34/2.42
Northern Telecom (GI)	65/125	-2.7	0.8	**

† Loss at test radius of 1mm.
* No measurable loss up to breaking radius.
** Data did not follow Equation 2.

SUMMARY OF MANDREL WRAP RESULTS
Table 1

The breaking radius, determined by the minimum radius that the fibre could withstand without breaking, is in the range 0.8 – 1.5 mm. This value sets a limit on the maximum distortion the fibre can tolerate and was used in the design of the grooved pressure blocks in the microbending sensor. The Sieverts-Ericsson step index fibre is unusual in that the fibre has a high index of refraction core, 1.54, with a large numerical aperture, ~0.6. While most fibres are coated with a soft polymer jacket, this fibre has a hard epoxy acrylate coating on top of the usual soft jacket. No attenuation losses were observed, even at the breaking limit. While this fibre has excellent microbending insensitivity, good for communication links, it would be a poor choice for sensing applications.

The prime thrust of this work was to capitalize on the properties of the soft polymer coating to distribute tensile loads so that the fibre could be bent repeatedly without failure. A coated Corning step index fibre was cycled many times with no evidence of any degradation, Fig 4. (upper curve). After removing the coating from a similar piece of optical fibre, the transducer had a catastrophic failure during the first cycle. This figure dramatically reveals the importance of fibre coating to sensor lifetime. In the periodically induced microbending geometry, the selection of the corrugated shape was critical. A sharp tooth design on cycling caused the coating to break down and rip away from the glass fibre. Any nicks generated by working soon caused the fibre to fail. In addition, fractures in the coating introduced undesirable hysteresis and hence irreproducibility into the transmission curves. After experimenting, grooved pressure blocks (Fig. 1) manufactured from polyethyl-vinylchloride (PVC) with a groove depth and ridge height of 1.6 mm, were chosen for the sensor.

The transmission loss curve, Fig. 5, for Corning Corguide step index fibres, demonstrates four distinct regions of response. A nonlinear response was observed as the corrugated jaws first bent the fibre. This was followed by two linear regions, then a saturation where most of the high angle modes were removed.

The two straight line regions have been identified as due to "slipping" at low distortions and "pinning" at high distortions. In the low region, the curved nature of the jaws allowed the fibre to slip between the teeth as the pressure was first applied. As the blocks moved closer, the frictional forces between the compliant coating and the blocks increased to a point where the fibre became pinned and the slipping was impeded. Thereafter the bending was purely elastic. The approach taken here to remove the slipping was to pretension the sensor head with loads in the range 0 to 4 N. The slipping region is now shifted out of range and a single linear response results, Fig. 6. In addition, the use of pretension increased the slope and hence the sensitivity. Best response curves occurred for pretensioning in the range 2.2 – 2.5 N.

Theory predicts that the amount of light attenuation depends on the length of the bent fibre; hence multiple bends should produce a larger dynamic range. The grooved pressure block has facilities to measure 1 to 4 bends and the distance between bends was 4.8 mm. Figure 7 shows how the dynamic range was increased for 1 to 3 bends. Little additional range was gained with a fourth bend. It appears that most of the rays closest to the critical angle have been shunted into leaky modes after 3 bends. It was also noted that hysteresis in the response curve reduced as the number of bends increased. It is suggested that for our mechanical periodicity, the parameters which affect hysteresis are random and this effect tends to be self-cancelling.

Summary

We have developed a wide range sensor using the principle of induced microbending losses. The performance of these devices depends critically on the selection of bending geometry and of materials. These devices have an optical dynamic range of 6 dB and a displacement sensitivity of 0.16% transmission/μm. Future work will incorporate these results into displacement, switch closure and pressure sensors.

Acknowledgments

The authors wish to acknowledge financial assistance from Focal Marine Limited in support of this project and one of us (KEL) is indebted to the above company for scholarship support.

References

1. Giallorenzi, T.G. et al.,"Optic Sensor Technology" IEEE J.Quant.Electr. QE-18 Vol.20 No.2, pp. 626-687. 1982.
2. First International Conference on Optical Fibre Sensors, Proceedings IEE April 1983.
3. De Paulo, R.P. and Moore, E.L., "Fibre Optic Sensor Overview" SPIE Proceedings on Fiber Optic and Laser Sensors III, pp. 2-15. 1985.
4. Bucaro, J.A., Dardy, H.D. and Carome, E.F,"Optical Fibre Hydrophone" Appl. Opt., Vol. 16, pp. 1302-1304. 1977.
5. Cole, J.H., Johnson, R.L., and Bhuta, P.G, "Fibre Optic Detection of Sound" J. Acoust. Soc. Am., Vol. 62, pp. 1136-1143. 1977.
6. Lagakos, N. et al. "Multimode Optical Fiber Displacement Sensor" Appl. Opt. Vol.20 No. 2, pp. 167-168. 1981.
7. Marcuse D., Theory of Dielectric Optical Waveguides, Academic, New York 1974.
8. Marvin, D.C. and Ives, N.A."Wide Range Fiber Optic Strain Sensor" Appl. Opt., Vol. 23, pp. 4212-4217. 1984.
9. Gloge,D., "Bending Losses in Multimode Fibers with Graded and Ungraded Core Index" Appl. Opt. Vol.11 No. 11, pp 2506-2513. 1972.

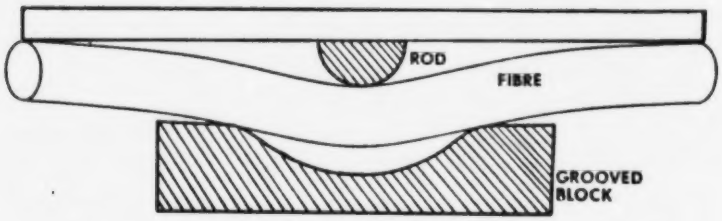

Figure 1. Grooved Block Design of Microbending Transducer.

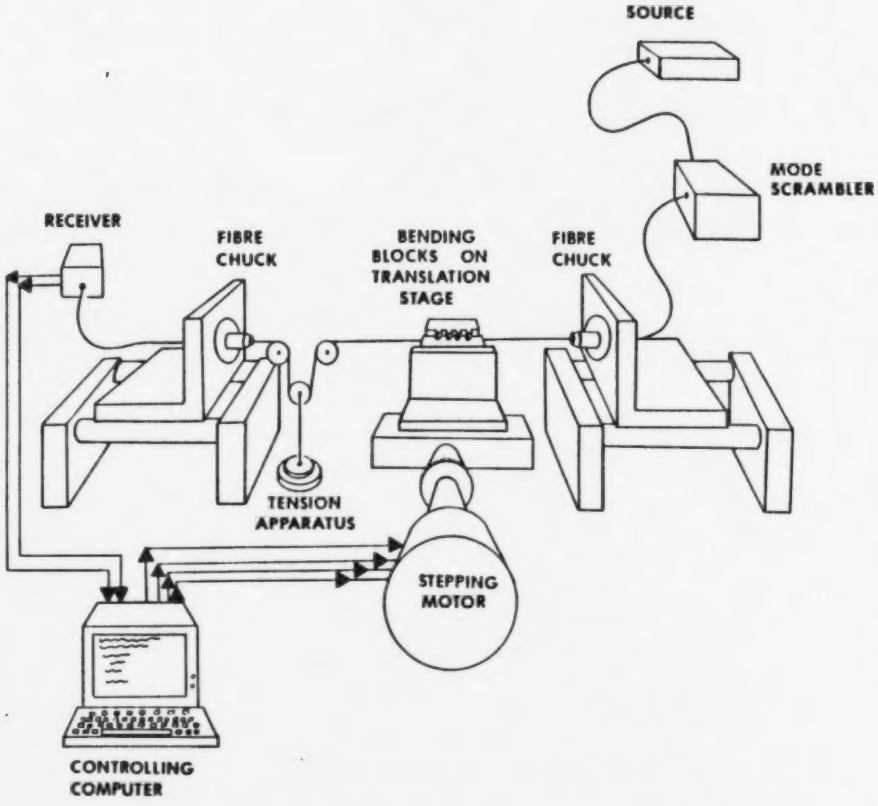

Figure 2. Experimental Arrangement for Investigating Microbending Losses.

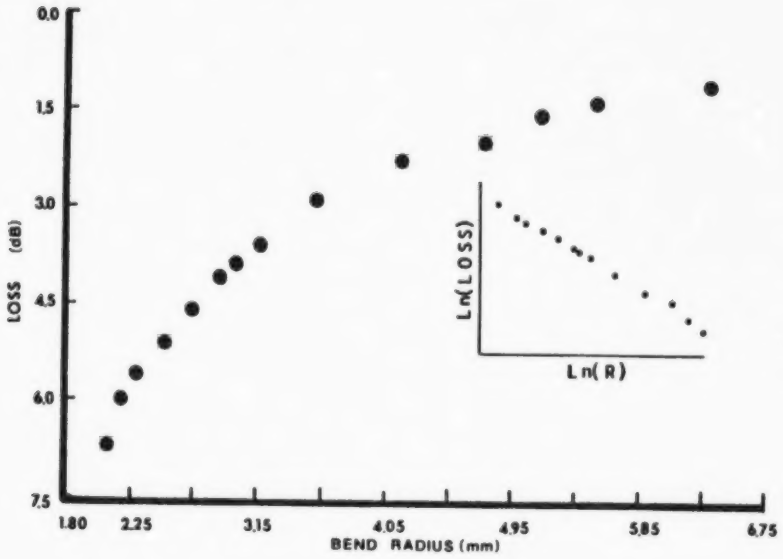

Figure 3. Bending Loss Curve for Corning Step Index Fibre. Inset shows excellent fit to Equation 2.

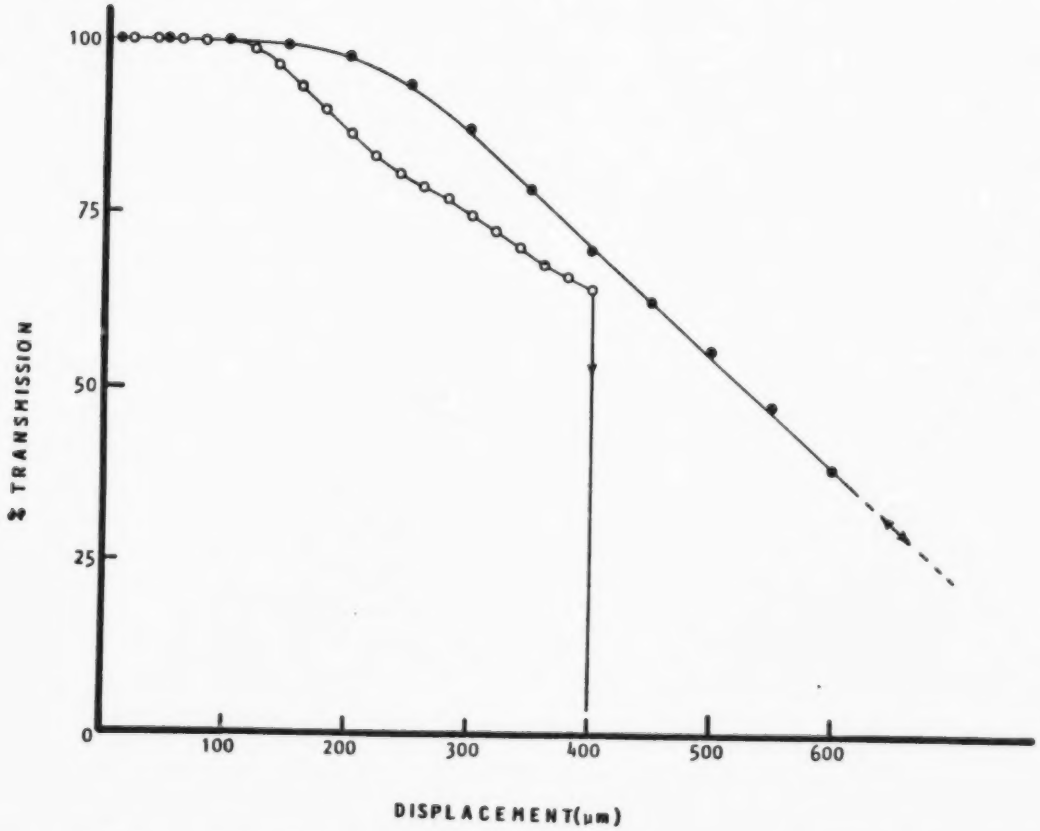

Figure 4. Response Curve for Coated and Non-coated Step Index Fibre on Cycling. On the first cycle the uncoated fibre demonstrated a catastrophic failure.

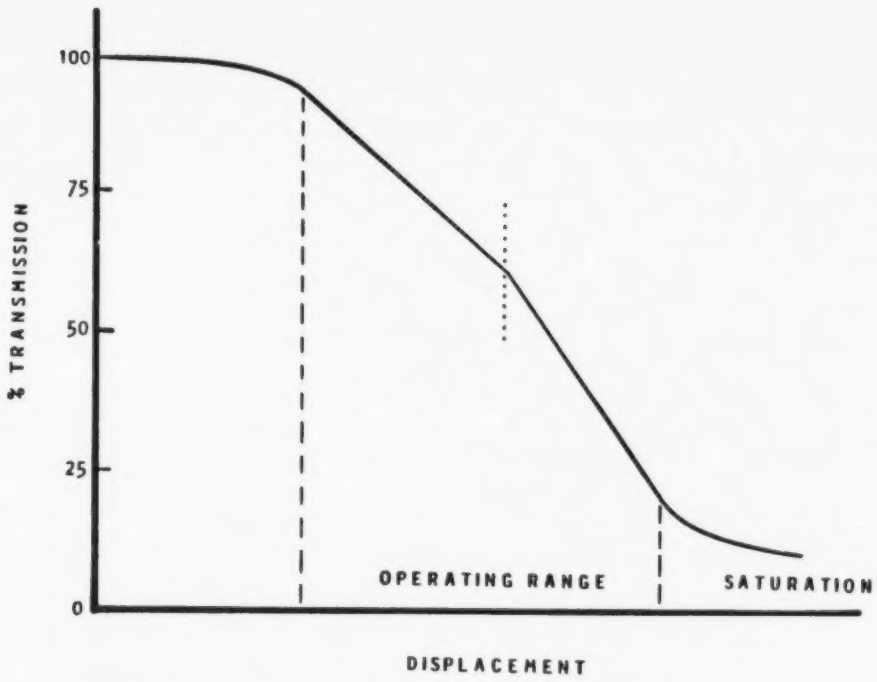

Figure 5. Response curve for Corning Corguide step index fibre displays four distinct regions. Note the two linear responses in the usual operating range.

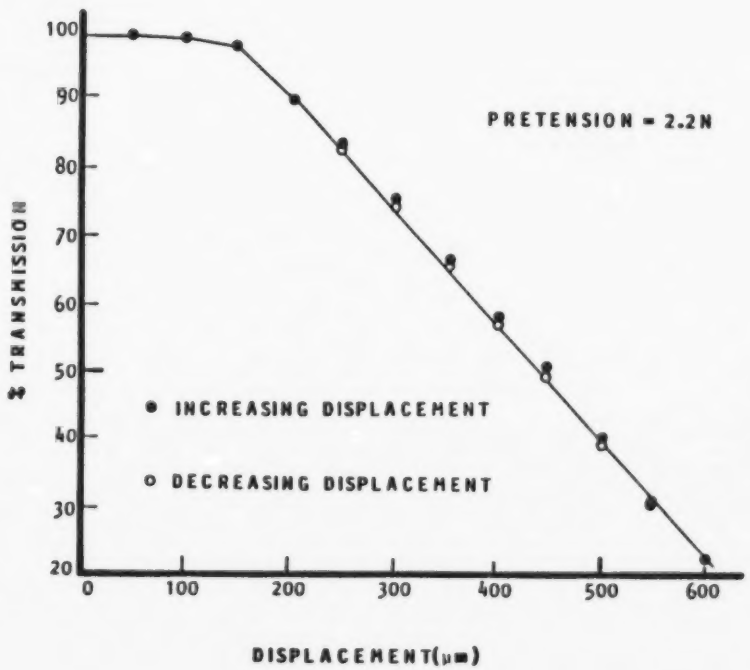

Figure 6. Microbending sensor with pretension yields a linear response. Residual hysteresis is indicated by the solid circles and the open circles.

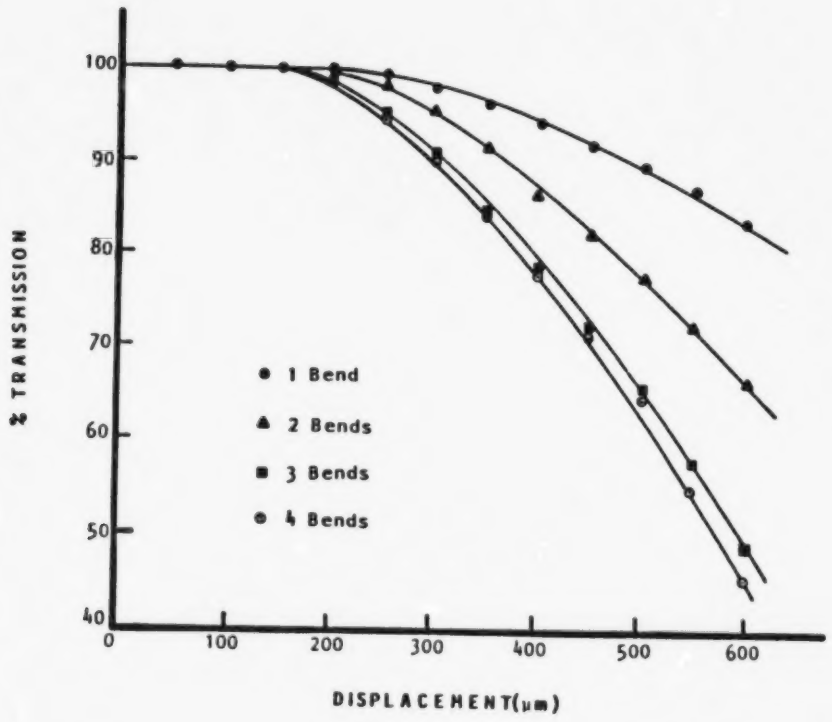

Figure 7. Effect of multiple bends on the optical transmission.